Impaired reliability and precision of spiking in adults but not juveniles in a mouse model of Fragile X Syndrome

Deepanjali Dwivedi [1], Sumantra Chattarji [1, 2, 3], Upinder S. Bhalla [1, 2]

[1] National Centre for Biological Sciences, TIFR, GKVK campus, Bellary Road, Bangalore 560065, India

[2] Centre for Brain Development and Repair, Institute for Stem Cell Biology and Regenerative Medicine, Bangalore 560065, India.

[3] Centre for Discovery Brain Sciences, Deanery of Biomedical Sciences, University of Edinburgh, Hugh Robson Building, 15 George Square, Edinburgh EH89XD, UK

Correspondence should be addressed to: Dr. Upinder S. Bhalla, National Centre for Biological Sciences, TIFR, GKVK campus, Bellary Road, Bangalore.

E Mail ID – bhalla@ncbs.res.in

Number of Pages : 65

Number of Figures : 9

Word Count

Abstract - 146, Introduction - 662, Discussion – 1939

Author Contribution DD and USB designed the project. SC and USB provided the animals and equipments for the project. DD did the experiments and the analysis. DD and USB wrote the paper.

All authors declare having no conflicts.

Abstract

Fragile X Syndrome (FXS) is the most common source of intellectual disability and autism. We report increased firing variability in pyramidal neurons in the CA1 of hippocampal slices from Fragile-X Mental Retardation Protein knockout (FMRP) mice in adults, but not juvenile mice. This increased spiking variability was correlated with reduced spike number and with elevated AHP, which arose from elevated SK currents. However, SK distribution was unchanged in mutants. We obtained a partial rescue of the cellular variability phenotype in CA1 when we blocked SK current using the specific blocker apamin. Further, we show a differential effect of FMRP Knock Out in different sub-regions of hippocampus in juvenile mice where we observed a significant change in spike numbers from pyramidal neurons in CA3, but not CA1. The present study provides single cell correlate of the network observations of response variability and loss of synchronization in FXS.

INTRODUCTION

Fragile X Syndrome (FXS) is an autism spectrum disorder arising from increased repeats of CGG tri-nucleotide in the FMR1 gene. This leads to silencing of the gene and hence the absence of the FMRP protein. (Lubs', 1969.; O'Donnell and Warren, 2002). FMRP is a transcription factor which affects multiple downstream genes including ion channels (Brown et al., 2001; Darnell et al., 2011). Studies have shown that absence of FMRP affects the functioning of ion channels either by regulating the number of channels (Meredith et al., 2007; Strumbos et al., 2010; Gross et al., 2011; Lee et al., 2011; Routh et al., 2013; Ferron et al., 2014; Zhu et al., 2018) or by directly interacting with the channels (Brown et al., 2010; Deng et al., 2013). Multiple studies have shown that potassium channels have a significant effect on spike precision (Fricker and Miles, 2000; Gittelman, 2006; Cudmore et al., 2010), and many of these potassium channels are transcription hits for FMRP. This leads to the hypothesis that FXS may alter the functioning of one or multiple potassium channels, leading to effects on spike precision.

In recent years a number of in-vivo hippocampal recording studies have shown that there is poor correlation of spiking activity between cells, and abnormal theta-gamma phase coupling in FXS mice (Radwan et al., 2016; Arbab et al., 2018, 2018; Talbot et al., 2018). In medial Prefrontal Cortex (mPFC), variability in calcium (Ca2+) responses has also been observed, leading to impaired Spike Timing Dependent Plasticity (STDP) (Meredith et al., 2007).These studies have led to the 'discoordination hypothesis' for FXS (Talbot et al., 2018). This hypothesis states that neurons in FXS are uncorrelated and have aberrant network discharges. In apparent contradiction to this hypothesis, neurons showed hyper connectivity and

synchronization in cortical networks of FXS model mice (Testa-Silva et al., 2012; Gonçalves et al., 2013)

Synchronicity is an emergent property of a network and is a function of both network connectivity and intrinsic properties. Specifically, potassium conductances have been shown to have significant effects on spike precision and network synchrony (Fricker and Miles, 2000; Pfeuty et al., 2003; Deister et al., 2009; Cudmore et al., 2010; Gastrein et al., 2011; Hou et al., 2012). Modeling studies have also shown that conductances which mediate spike frequency adaptation help to synchronize network firing (Crook et al., 1998). I_h currents, I_M currents and SK currents have been shown to mediate adaptation for phase precession in hippocampal neurons (Orban et al., 2006; Kwag et al., 2014), spiking reliability in insect neurons (Gabbiani and Dewell, 2018) and also to maintain regular firing in robust nucleus of acropallium in zebra finches (Hou et al., 2012). Thus FXS mutations, through their effects on potassium channels, may lead to several of the observed network dysfunctions in FXS models.

In the present study we tested if there were single cell mechanisms that might underlie the above network observations of uncorrelated activity. First, we observed that cells from FXS knockout (KO) hippocampal slices were more unreliable and imprecise than controls. Consistent with the developmental manifestations of FXS, this effect was absent in juvenile mice and emerged only after ~6 weeks. Decreased spiking in KO mice was correlated with increased variability. At the mechanistic level, we found that the spiking changes were due to elevated medium AHP (mAHP) which in turn was due to elevated SK currents. In contrast to these observations of decreased spiking in the CA1 region of adult animals, we observed increased spiking in the CA3 region of juvenile animals (as seen in Deng et al., 2018) but not in CA1.

We did not see any significant change in spatial distribution of SK channels either in CA3 or CA1, in either juvenile animals or in adult animals. This too is consistent with earlier observations (Deng et al., 2018). Finally, we tested the outcome of blockers of SK and found that that they indeed led to a partial rescue of the observed phenotype of increased spiking variability in adult animals.

RESULTS

FMR1 KO cells exhibit increased variability in spike numbers and impaired spike precision

We performed whole cell patch clamp recordings in brain slices from CA1 cells of dorsal hippocampus in wild-type (WT) and KO littermate animals (6-8weeks old). Somatic current injection was used to inject various waveforms of current (Fig 1A). These included a square current step, frozen noise riding on a current step, and a sinusoidal waveform riding on a current step. In each case we measured the variability in spiking over the 900 ms of current injection, in two respects: first, the variability within a neuron, over repeated trials (CV_w), and second, the variability between neurons, comparing matching trials between cells (CV_b).

We computed the co-efficient of variation (CV) of spike numbers for each of the current stimulus protocols (methods). We observed that the CV of spike numbers across trials within cells (CV_w) was significantly higher for KO cells as compared to WT, but only for the step current protocol (CV_w for WT 0.038 ± 0.005, n=30 cells; CV_w for KO 0.057 ± 0.006, n=29 cells; p=0.0048, Wilcoxon rank sum test) (Fig 1E). For other protocols, where frozen current noise or sinusoidal waveforms were riding on top of a current pulse, spikes were very reliable over different trials for both WTs and KOs. (Fig 2A, Fig 2B, Fig 2C, Fig 2D and Fig 2E). We then estimated the variability between cells (CV_b). To do this, we compared spike numbers between WT and KO by matching corresponding trials, such that we compared spiking between the first trial of WT and the first trial of the KO recording, the second trial of WT with

the second trial of KO, and so on. From this procedure we found that between cell variability was significantly elevated in KO cells as compared to WT (CV_b for WT cells 0.29 ± 0.003, n=30 cells; CV_b for KO cells 0.41 ± 0.002, n=29 cells. $p<0.001$; Wilcoxon rank sum test) (Fig 1F).We plotted the CV_w of spike numbers within the cell, for WT and KO population and observed that KOs have much wider spread as compared to WT (SD of the CV_w population for WT cells = 0.026, n=30 cells; SD of the CV_w population for KO cells = 0.03, n=29 cells) (Fig 1G and 1H). This implied that KOs have a more heterogeneous population than WT cells. In KO mice, some cells are reliable and they produce similar number of spikes across multiple trials but some did not.

Spike precision was computed by finding jitter in spike times for the current step input protocol (methods). Jitter in spike times increased over the time course of each trial (Fig 1I, Fig 1J), and this increase was significantly larger in KOs as compared to WT mice (Slope 0.04 ± 0.002 for WT, n=30 cells; Slope 0.06 ± 0.006, n=29 cells for KO; p=0.031; Wilcoxon rank sum test) (Fig 1J). This implies that in addition to increased within cell (CV_w) and between cell (CV_b) variability of spike numbers, spikes produced by KO cells are also imprecise in their timing. Such variable spiking behavior and imprecise spike timings are both indicative of abnormal coding abilities in KO neurons. Thus these initial recordings showed that there was increased heterogeneity in spiking in CA1 pyramidal neurons of KO mice

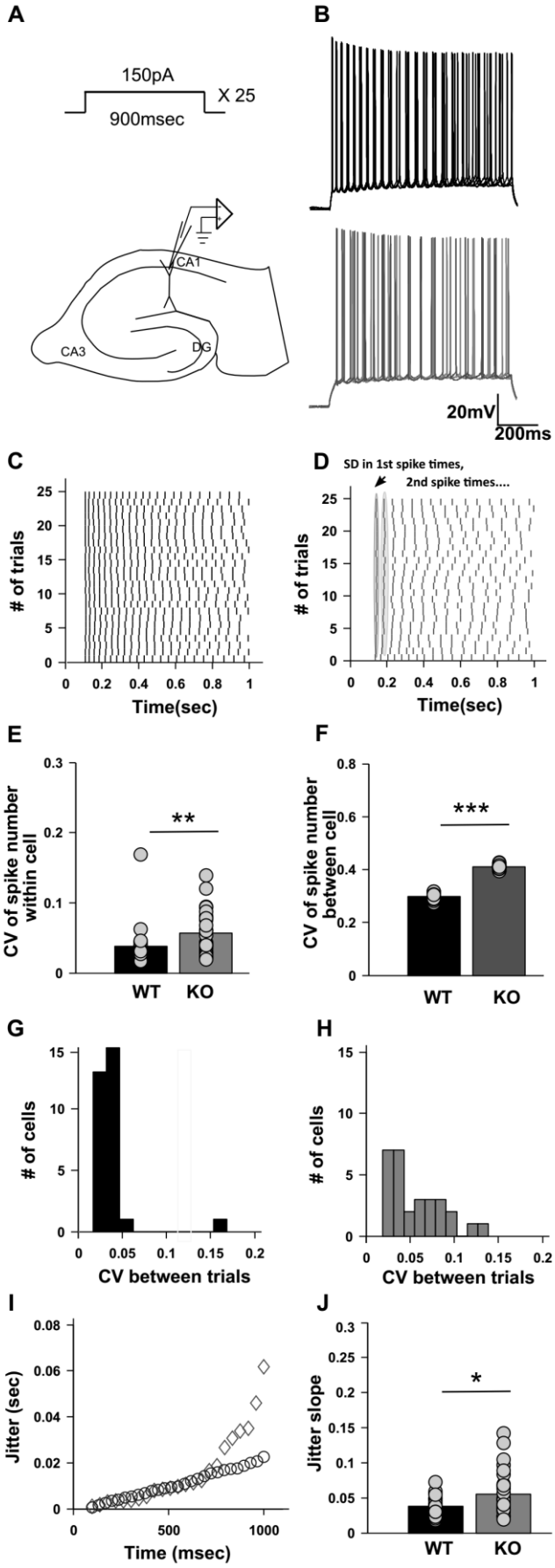
A
150pA
X 25
900msec
CA1
CA3
DG
B
20mV
200ms
C
# of trials
Time(sec)
D
SD in 1st spike times,
2nd spike times....
# of trials
Time(sec)
E
CV of spike number within cell
**
WT
KO
F
CV of spike number between cell
***
WT
KO
G
# of cells
CV between trials
H
# of cells
CV between trials
I
Jitter (sec)
Time (msec)
J
Jitter slope
*
WT
KO

162

Figure 1. Increased spike variability and spike timing imprecision both at within cell level (CV_w) across multiple trials and between cells (CV_b) in CA1 hippocampus of FXS animals.

(A) Schematic of a hippocampal slice and the step depolarization protocol. The protocol consists of a 150pA step for 900msec time duration repeated over 25 trials.

(B) Representative raw traces of spiking, superimposed for four trials only for WT (black) and KO (grey). Scale bar 20mV, 200msec.

(C) Representative raster plot showing spiking for the step depolarization protocol for WT (black) and (D) KO (grey). Also showing the methodology for computing jitter slope for estimating spike timing precision, further plotted in 1G and 1H.

(E) Bar plot for within cell variability across multiple trials (CV_w) WT (n=30 cells, black) and KO (n=29 cells, grey). KO cells have significantly higher within cell variability than WT cells (p=0.0048, Wilcoxon rank sum test).

(F) Bar plot for between cell variability (CV_b) for matched trials, WT (n=30 cells, black) and KO (n=29 cells, grey). KO cells have significantly higher between cell variability than WT cells (p<0.001, Wilcoxon rank sum test)

(G) Histogram showing spread of CV_w parameter for WT (n=30 cells, black) and (H) for KO. KO cells have more spread in CV_w parameter, depicting heterogeneity in KO cell population.

(I) Representative trace showing jitter in spike timings for WT (n=30 cells, black circles) and KO (n=29 cells, grey diamonds). Jitter in spike timings increases in the later part of the trial, in a 900mec trial period.

(J) Bar plot for jitter slope, a measure of spike precision for WT (n=30 cells, black) and KO (n=29 cells, grey). Jitter slope is significantly higher for KO cells as compared to WT depicting impaired spike timing precision over multiple trials (p=0.031; Wilcoxon rank sum test).

KO mice exhibit increased variability in spike number between cells (CV_b) for frozen noise stimuli

Neuronal coding takes place against a noisy background of continuous synaptic input (Faisal et al., 2008). Frozen noise stimuli have therefore been used in several studies to examine single-neuron computations and are considered more physiological (Stevens and Zador, 1998; Carandini, 2004; Fujisawa et al., 2004; Han and Boyden, 2007). We injected noise waveforms in the soma using a design similar to that of Mainen and Sejnowski, 1995. The stimulus waveforms were mainly either of random noise or sinuosoidal input currents (for details see methods). For noisy inputs, spikes across multiple trials aligned very precisely for both WT (Fig 2A, 2C) and KO cells (Fig 2B, 2D). Upon computation of CV of spike numbers across trials within cell (CV_w), there were no statistically significant differences for any of the protocols (Fig 2E). However, between cell variability differences (CV_b) were still significantly elevated for KO cells, for all stimulus protocols (Fig 2F). We did three way ANOVA for all the protocols on the no of spikes produced in respective protocols for WT and KO. The 3 factors were: across trials, across cells and WT vs.

KO. ANOVA results were significant for across cells ($p<0.001$), for WT vs. KO ($p<0.001$) but not for across trials ($p=1$) for all the protocols. Thus, between cell variability (CV_b) are robust phenotypic differences which manifest for the input noise stimulus as well. The same is not true for across trials within cell (CV_w) differences.

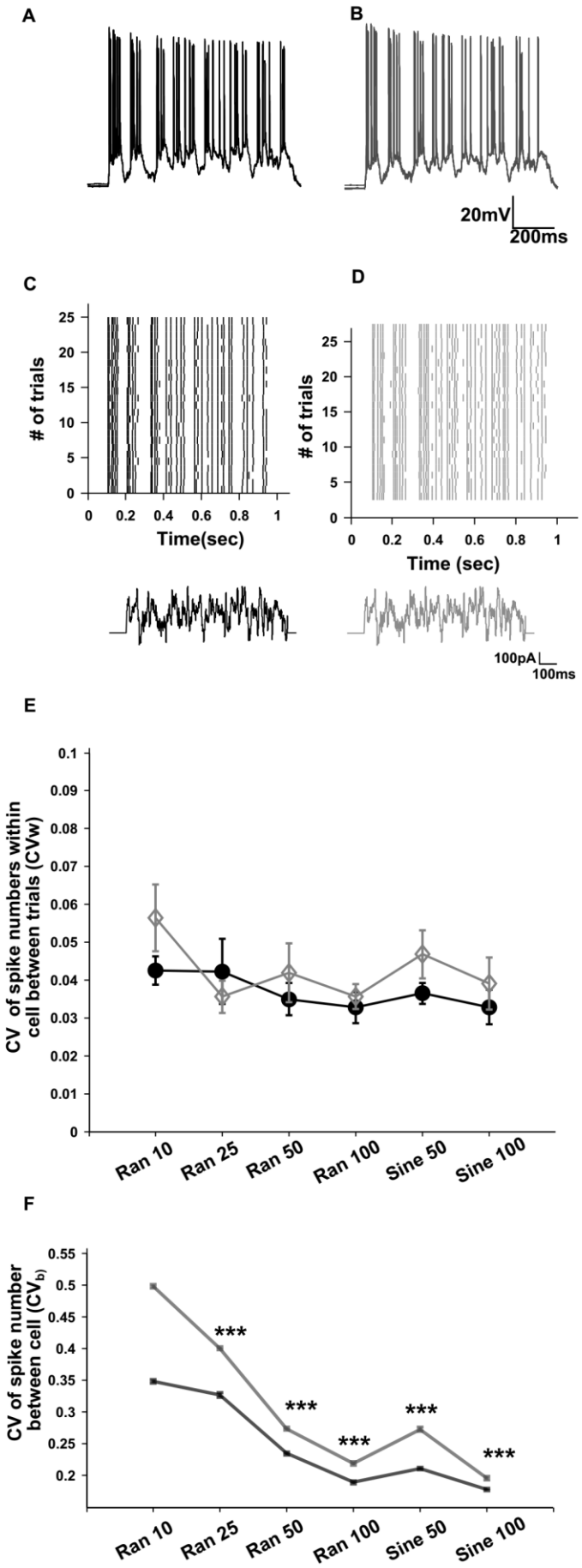
A
B
20mV
200ms
C
D
# of trials
Time(sec)
Time (sec)
100pA
100ms
E
CV of spike numbers within cell between trials (CVw)
Ran 10
Ran 25
Ran 50
Ran 100
Sine 50
Sine 100
F
CV of spike number between cell (CVb)
***

215

Figure 2. KO cells have increased spike variability between cells (CV_b) for noise and sinusoidal stimuli but not for within cell variability (CV_w) across trials.

(A) Representative raw plot of spiking showing no spike variability or spike precision differences for Random 100 noise protocol across multiple trials for WT and (B) for KO. The trace is for four superimposed trials. Scale bar 20mV, 200msec.

(C) Raster plot showing no spike variability or spike precision differences for Random 100 noise protocol across multiple trials for WT and (D) for KO. Trace below indicates Random 100 input protocol. Scale bar 100mV, 100msec

(E) Line plot for within cell variability differences (CV_w) for all noise and sinusoidal protocols for WT (filled black circles) and KO (grey diamonds). The protocol is numbered by the standard deviation (SD) in pA (random protocols) or sine-wave amplitude (sine protocols) (Random 10 protocol: n=16 for WT and n=13 for KO; Random 25: n=16 for WT and n=13 for KO; Random 50: n=10 for both WT and KO; Random 100: n=10 for both WT and KO; Sine 50: n=10 for both WT and KO; Sine 100: n=10 for both WT and KO; error bar represent SEM). No significant within cell variability (CV_w) differences were seen between WT and KO in any protocol.

(F) Line plot for between cell variability differences (CV_b) for all noise and sinusoidal protocols (Random 10 n=16 for WT and n=13 for KO; Random 25 n=16 for WT and n=13 for KO; Random 50 n=10 for both WT and KO; Random 100 n=10 for both WT and KO; Sine 50 n=10 for both WT and KO; Sine 100 n=10 for both WT and KO). Significant differences were seen ($p < 0.001$; three-way ANOVA, error bar represent SEM) for all pairs.

Spike imprecision diverges between KO and WT only in adult mice

Fragile X is known to have an age dependent effect where some disease phenotypes get worse with age (Larson, 2005; Cornish et al., 2008; Choi et al., 2010). We asked if similar effects of age might manifest in the phenotype of firing imprecision of KO cells. We therefore repeated our experimental protocols in 3-4 week old WT and KO littermate mice. Regular spike firing was observed in both KO and WT cells for step input current injection. As before, we assessed variability of spike numbers across multiple trials for within the cell (CV_w).There was no significant difference between WT vs. KO in these younger mice (CV_w for WT 0.04 ± 0.009, n=12 cells; CV_w for KO 0.03 ± 0.004,n=10 cells; p=0.81; Wilcoxon rank sum test) (Fig 3A,3B,3C,3D and 3E).Spike precision was also assessed as above, by finding the slope for spike jitter. By this measure too, spike timings were not significantly more imprecise for KO as compared to WT (Slope for WT younger 0.05 ± 0.01, n=12 cells; Slope for KO younger 0.04 ± 0.003, n=10 cells; p=0.9; Wilcoxon rank sum test) (Fig 3F). We further observed that the CV_w of spike number was significantly higher in older KOs as compared to younger KOs (CV_w for KO older 0.057 ± 0.006, n=29 cells; CV_w for KO younger 0.03 ± 0.004, n=10 cells; p=0.01, Wilcoxon rank sum test) (Fig 3E). However CV_w was not a function of age for WT animals (CV_w for WT older 0.038 ± 0.005, n=30 cells; CV_w for WT younger 0.04 ± 0.009, n=12 cells; p=0.38, Wilcoxon rank sum test) (Fig 3E). Similar effects were

seen using our analysis of jitter in spike timing. Spike timing jitter was significantly higher for older KO animals as compared to younger KO animals (Slope for KO older animals 0.06 ± 0.006, n=29 cells; Slope for KO younger animals 0.04 ± 0.003, n=10 cells; p= 0.04; Wilcoxon rank sum test) (Fig 3F) but such divergence with age was not seen for WT animals. (Slope for WT older animals 0.04 ± 0.002, n=30 cells; Slope for WT younger animals 0.05 ± 0.01, n=12 cells; p=0.75, Wilcoxon rank sum test) (Fig 3F). A two way ANOVA was done on the spike numbers where the two factors were: between different ages of the animals and WT vs. KO. There was a non significant change between ages of the animals for both WT and KO ($F_{(1,78)}$= 0.96; p=0.7) but there was a significant reduction in spike number for KO animals as compared to WT ($F_{(1,78)}$=5.1; p=0.027) (Fig 3G). However, the frequency-vs.-current (f-I) curves were not significantly different between WT and KO either in the older (8 weeks) or younger (4 weeks) age groups (Mean gain for f-I curve older WT 0.16 ± 0.007 spikes. s^{-1} . pA^{-1} , n= 27 cells; mean gain for f-I curve older KO 0.16 ± 0.008 spikes. s^{-1} . pA^{-1}, n= 25 cells; p=0.96 Wilcoxon rank sum test; Mean gain for f-I curve younger WT 0.13 ± 0.01 spikes. s^{-1} . pA^{-1}, n=12 cells; mean gain for f-I curve younger KO 0.13 ± 0.01 spikes. s^{-1} . pA^{-1}, n=10 cells; p=0.1; Wilcoxon rank sum test) (Fig 3I and 3J). Other properties like spike threshold were also not significantly different between WT and KO (Spike threshold for the 1st spike WT -53.6 mV ± 0.56 n=30 cells; spike threshold for 1st spike KO -53.8 mV ± 0.62, n=29 cells; p= 0.87; Wilcoxon rank sum test; Spike threshold for the last spike WT -41.9 mV ± 0.66, n=30 cells; Spike threshold for the last spike KO -43.5 mV ± 0.66, n=29 cells, p=0.1; Wilcoxon rank sum test). The spread in number of spikes produced by KO neurons was greater than observed in WT, further substantiating the point of increased variability in KO neurons (SD of spike numbers WT 7.2; n=750 spikes from 30 cells

25 trials each; SD of spike numbers KO 8.1; n=725 spikes from 29 cells 25 trials each)(Fig 3H). We performed a 3-way ANOVA in which the factors were: across trials, across cells, and WT vs. KO for older age group data. The ANOVA results were highly significant for variability in spike numbers between cells (CV_b) ($F_{(29,1420)}$=32.04 , $p<0.001$) and differences in spike numbers between WT and KO for older animals ($F_{(1,1420)}$=209.9, $p<0.001$) but across-trial comparisons did not exhibit a significant difference ($F_{(24,1420)}$=0.15, p=1).Thus, there is increase in spike variability with lowered spiking precision for juvenile KO mice as compared to adult KO mice. This divergence which is observed for KO animals with age does not happen for WT animals.

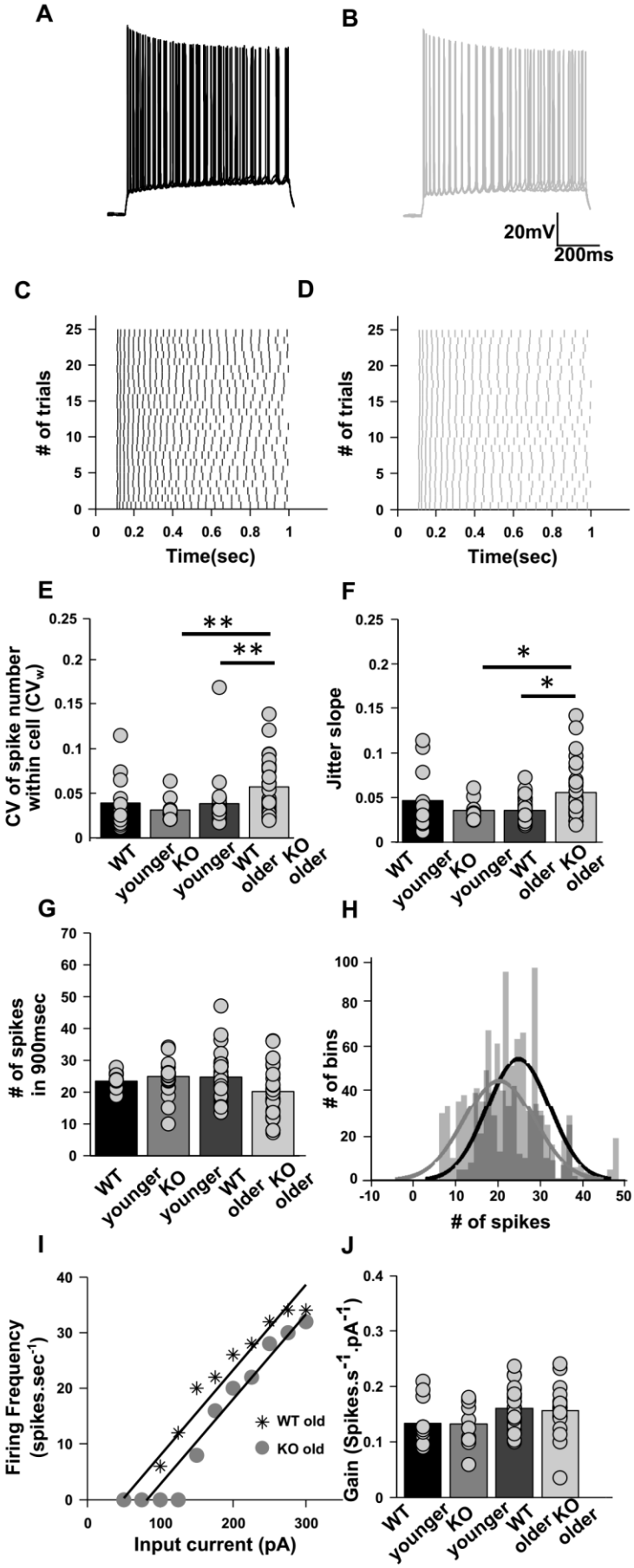
A
B
20mV
200ms
C
D
# of trials
Time(sec)
E
F
CV of spike number within cell (CVw)
Jitter slope
WT younger
KO younger
WT older
KO older
G
H
# of spikes in 900msec
# of bins
# of spikes
I
J
Firing Frequency (spikes.sec-1)
Input current (pA)
WT old
KO old
Gain (Spikes.s-1.pA-1)

302

Figure 3. Spiking variability and spike imprecision diverges in adult KO animals as compared to younger KO but not in WT.

(A) and (B) Representative raw traces of spiking, superimposed for four trials only for WT (black) and KO (grey). Scale bar 20mV, 200msec.

(C) and (D) Representative Raster plots showing spiking for the step depolarization protocol for WT younger (black) and KO younger (grey). Spikes align precisely and have low within cell variability (CV_w) across trials for KO younger as compared to WT younger.

(E) Bar plot for comparing within cell variability (CV_w) across multiple trials between WT younger (n=10 cells, black), KO younger (n=12 cells, grey), WT older (n=30 cells, light black) and KO older (n=29 cells, light grey). Spiking variability significantly increases for KO animals with age but not for WT animals (p=0.01, Wilcoxon rank sum test).

(F) Bar plot for jitter slope, a measure of spike precision for all groups as mentioned in (E). Spiking precision significantly decreases for KO animals with age but not for WT animals (p= 0.04; Wilcoxon rank sum test).

(G) Comparison of number of spikes produced during the 900msec stimulus period for each of the groups in (E). There is a non significant change in spike number with age in WT or KO (p=0.7; two way ANOVA) but there was a significant reduction in spike number for KO animals as compared to WT (p=0.027; two-way ANOVA).

(H) Superimposed histograms for number of spikes produced for WT (light grey) and for KO (dark grey). The plot shows greater spread in spike numbers produced in given trials for KO as compared to WT (p<0.001; three way ANOVA).

(I) Illustrative f-I curves for a representative cell from older (>6 week) WT animals (black stars), and a cell from older KO animals (filled grey circles). The gain (i.e., slope) for each cell was computed using a regression fit in the roughly linear domain between 50pA to 300pA (n=27 cells for WT older and n=25 cells for KO older).

(J) Gain computed by fitting a regression line through the f-I curve for each cell as illustrated in (G), for each of the four experimental conditions. The cells were the same as in G. The gains are not significantly different between WT and KO in any age group (n=27 cells for WT older and n=25 cells for KO older; p=0.96; Wilcoxon rank sum test; n=12 cells for WT younger and n= 10 cells for KO younger; p=1; Wilcoxon rank sum test).

Differential effect of FMRP KO in different brain regions

Mouse models of FXS are known to exhibit increased excitability (Contractor et al., 2015a; Deng and Klyachko, 2016; Luque et al., 2017). In contrast to previous studies, we observed that excitability was reduced in CA1 neurons in adult mice but not in juveniles. Deng et. al. 2019 have observed increased CA3 excitability in juveniles which was in contrast to what is we observed in CA1, namely, that there is no significant effect on excitability of CA1 pyramidal cells at this time point. In order to address this contrasting result, we repeated the protocol from Deng et. al. in our FXS model, and compared outcomes between CA3 and CA1 (Figure 4). In agreement with their study we observed significantly increased spiking in CA3 cells of FXS mice for some of the input holding currents (Figure 4 A, B). (# of spikes in 60 s for -48mV holding potential for WT 131.9 ± 17.42, n=10 cells; # of spikes in 60 s for

-48mV holding potential for KO 186.3 ± 27.27, n=10 cells; F ($_{1,72}$)=5.35, p=0.023 for difference between WT and KO; two-way ANOVA). We did similar experiments in CA1 pyramidal cells, using the protocol mentioned in Fig 3G and 3H, there was no difference in excitability between WT and KO (Figure 4 C,D; # of spikes in 60 s for -48mV holding potential for WT 355.58 ± 40.93, n=12 cells; # of spikes in 60 s for -48mV holding potential for KO 358.67 ± 22.56, n=12 cells; F($_{1,88}$)=1.06, p=0.31 for difference between WT and KO, two-way ANOVA). We therefore are able to replicate previous observations, and further find that there are contrasting effects of FMRP KO on the spiking properties CA1 and CA3 pyramidal neurons.

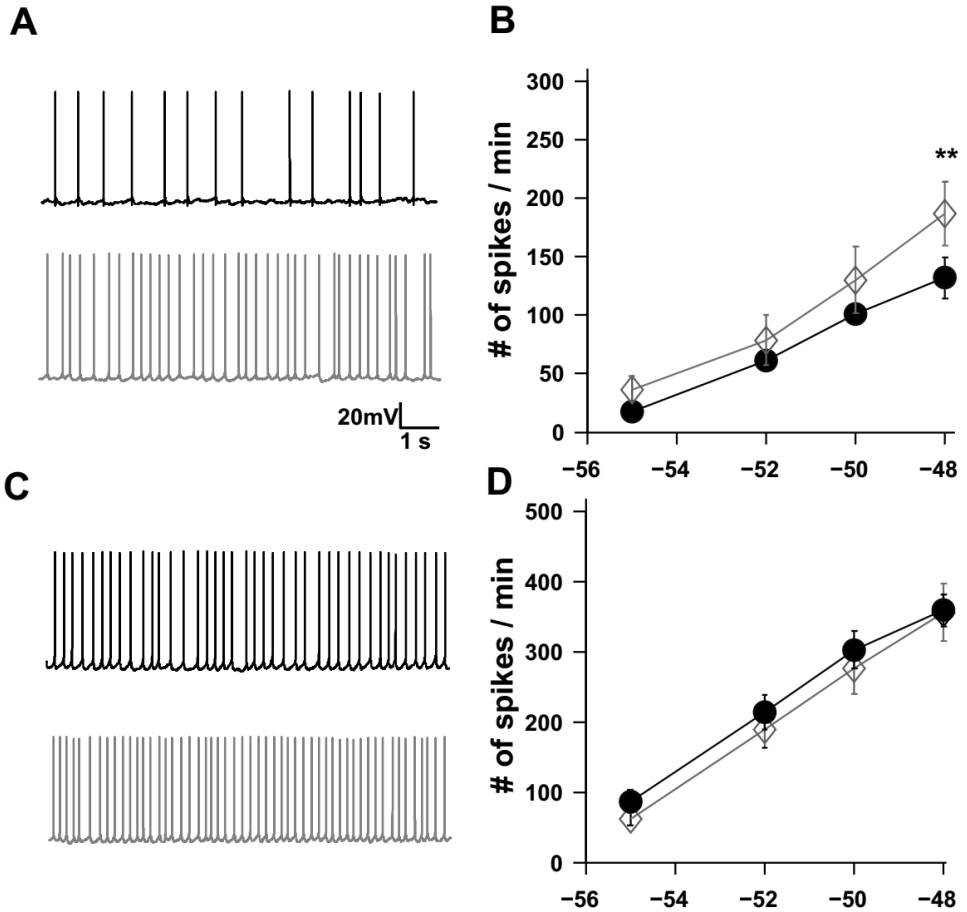

Figure 4. Contrasting effects of FMRP KO in different regions of hippocampus

A) Representative traces showing increased excitability between WT (upper trace, black) and KO (lower trace, grey) CA3 cells. Above traces are from the recording where the cells are held at -48mV. Scale bar 20mV, 1s.

B) Line plot showing increased excitability for KO CA3 cells (n=10 cells, grey diamond) as compared to WT CA3 cells (n=10 cells, filled black circles), when the cells were held at -48mV. For other holding potentials the spike numbers are not significantly increased for KO cells ($F(_{1,72})$=5.35, p=0.023 for difference between WT and KO, two way ANOVA, error bar represent SEM)

C) Representative traces showing no change in excitability between WT (upper trace, black) and KO (lower trace, grey) CA1 cells. Above traces are from the recording where the cells are held at -48mV. Scale bar 20mV, 1s.

D) Line plot showing no change in excitability for KO CA1 cells (n=12 cells, grey diamond) as compared to WT CA1 cells (n=12 cells, filled black circles) ($F(_{1, 88})$ =1.06, p=0.31 for difference between WT and KO, two-way ANOVA, error bar represent SEM).

mAHP currents are elevated in older KO animals as compared to WT but no significant changes in I_h and M currents

We next investigated the mechanisms for increased variability in KO animals, guided by the above observations of increased variability and fewer spikes (Fig 3G) in the later part of the current pulse. In particular, we hypothesized that medium afterhyperpolarization (mAHP) and slow afterhyperpolarization (sAHP) currents were likely candidates to mediate such slower-onset effects. We asked if these currents might be altered in FXS cells.

To test this hypothesis we compared AHPs for WT vs. KO in older and younger animals. Cells were held at -70mV to record AHPs. We quantified AHPs by examining the hyperpolarization elicited with a spike train of 5 spikes in 100msec. Hyperpolarization was quantified at mAHP peak (50msec after the spike train) and at sAHP peak (200msec after the spike train). In brief, we found that sAHP was elevated in both older and younger KOs, but mAHP was elevated only in older KOs. Both mAHP and sAHP were found to be elevated in older KO animals (mAHP for WT -0.26 ± 0.16,n=10 cells; mAHP for KO -0.71 ± 0.15,n=12 cells; p=0.02; Wilcoxon rank sum test; sAHP for WT 0.006 ± 0.1, n=10 cells; sAHP for KO -0.37 ± 0.11,n=12 cells; p=0.02; Wilcoxon rank sum test) (Fig 4C and Fig 4D). However, only sAHP but not mAHP was found to be elevated in younger KO animals (mAHP for WT younger 0.41 ± 0.2, n=11 cells; mAHP for KO younger -1.14 ± 0.5, n=16 cells; p=0.1; Wilcoxon rank sum test; sAHP for WT younger 0.04 ± 0.12, n=11 cells; sAHP for KO younger 0.047 ± 0.2, n=16 cells; p=0.04; Wilcoxon rank sum test)(Fig 4C and 4D. As there was no significant difference in spike variability and spike time precision in younger KO animals, we hypothesized that the observed spiking variability in older KO animals might be due to elevated mAHP currents.

The mAHP in CA1 cells is mediated by $\mathbf{I_h}$, M and SK currents. A previous study has shown that $\mathbf{I_h}$ currents are not significantly altered in soma of FXS cells (Brager

et al., 2012). M currents are known to affect the Resting Membrane Potential (RMP) and spike adaptation index (Madison et al., 1987; Guan et al., 2011; Nigro et al., 2014; Hönigsperger et al., 2015). Neither RMP nor spike adaptation index were significantly changed in FXS cells, indicating that M currents might not be responsible for the observed phenotype. To further test this idea, $\mathbf{I_h}$ currents and M currents were recorded from soma of CA1 cells and compared between WT and KO for adult animals. As there was no difference in mAHP at juvenile stage for KO cells, we did not measure I_h and M currents for them. $\mathbf{I_h}$ currents were recorded using a hyperpolarization pulse. The sag produced in response to the pulse, was quantified according to a method adapted from Brager and Johnston, 2012 (Methods, Fig 5E). As observed previously, there was no significant difference in $\mathbf{I_h}$ sag between WT and KO CA1 cells, at somatic level. (% sag for WT 17.7 ± 1.64, n=10 cells; % sag for KO 18.87 ± 2.51, n=10 cells; p=0.91; Wilcoxon rank sum test) (Fig 5F).

To measure M currents we used the protocol adapted from Shah et al 2002 (Methods). According to the protocol the cells were held at -20mV and M currents were deactivated in steps from -20mV to -80mV. M current specific toxin XE991 was used to obtain the post toxin trace. Post toxin trace was subtracted from pre toxin trace to obtain XE991 sensitive M currents (Fig 5G). We found no significant differences in M currents between WT and KO CA1 cells. (Mean M current for step -80mV for WT -40.9 ± 6.33, n=19 cells; Mean M current for step -80mV for KO 45.94 ± 6.87, n=19 cells; $F_{(1,252)}$, p=0.11 between WT and KO, two-way ANOVA) (Fig 5H). Overall, these observations suggest that neither Ih nor M currents contribute to the observed elevation in mAHP in KO animals.

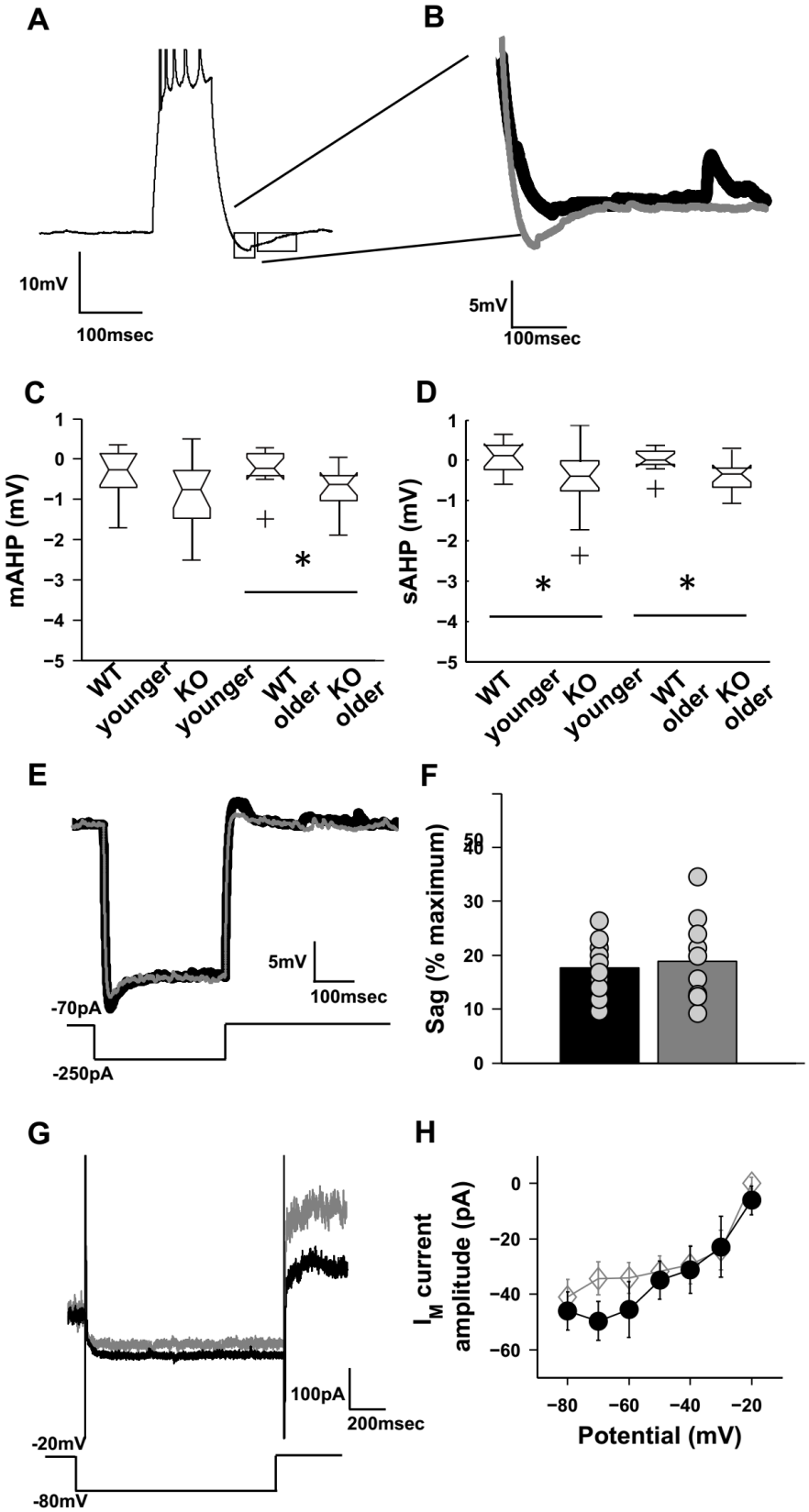

Figure 5. mAHP and sAHP are elevated in FXS KO neurons

(A) Representative trace for the protocol to measure mAHP and sAHP. Hyperpolarization within 50msec of the spike train (1) is quantified as mAHP while hyperpolarization following the spike train 200msec after the spike train (2) is quantified as sAHP. Scale bar 10mV, 100msec.

(B). Superimposed traces of WT older and KO older AHP currents showing elevated mAHP currents for KO cell (grey) as compared to WT cell (black). Scale bar 5mV, 100msec.

(C) Box plot showing mAHP currents for all groups (n=10 cells for WT older, n=12 cells for KO older, n=11 cells for WT younger and n=16 cells for KO younger). mAHP are elevated only for older KO animals vs. older WT 9 (p=0.02; Wilcoxon rank sum test, error bar represent SEM).

(D) Box plot showing sAHP currents for all groups (n=10 cells for WT older, n=12 cells for KO older, n=11 cells for WT younger and n=16 cells for KO younger). sAHP is elevated for both older KO vs. older WT and younger KO vs. younger WT (p=0.02; Wilcoxon rank sum test, error bar represent SEM).

(E) Representative trace for the protocol to measure I_h current. Superimposed traces of WT (black) and KO (grey) showing no significant difference in the response. Sag produced in response to 250pA hyperpolarizing pulse was quantified to estimate I_h current. Scale bar 5mV, 100msec.

(F) Box plot for showing %sag produced due to I_h current for WT older and KO older (n=10 cells for both WT and KO older). There was no significant difference in sag due to Ih current (p=0.91, Wilcoxon's test).

(G) Representative traces showing XE991 sensitive M current for WT older (black) and KO older (grey). The traces were plotted by finding the difference between pre

and post toxin current trace for input step from -20mV to -80mV. Scale bar 100pA, 200msec.

(H) Line plot showing IV curve of XE 991 sensitive M current. There is no significant difference in the M currents between WT older (filled black circles) and KO older (grey diamond) for any of the input steps. (n=19 cells for both WT and KO, $F_{(1,252)}$ = 2.5, p=0.11 between WT and KO, two-way ANOVA,error bars represent SEM)

SK currents are elevated in older KO animals as compared to WT

SK currents are also known to contribute substantially to mAHP (Sah and Clements, 1999, Stocker et. al 1999). It has also been shown that Ca2+ influx from VGCCs is elevated in FXS cells (Deng et al., 2011, 2013), indicating elevated Ca2+ levels intracellularly and hence increased SK channel activation. Thus, we hypothesized that SK currents are elevated in FXS cells, leading to the observed elevated mAHP in these cells. To test this, we used a procedure from Carlen, 1997. Outward currents were evoked using step depolarization of the cell from -55mV to +5mV and above (Fig 5A and 5B), in voltage clamp mode. Apamin was bath applied to obtain post apamin trace. The difference current of pre apamin and post apamin was quantified as SK currents. These currents were significantly higher in KO animals as compared to WT for adult age group (SK current for older WT at +15mV

step 54.2 ± 9, n=13 cells; SK current for older KO at +15 mV step 131.73 ± 25.5, n=13 cells; $F_{(1,240)} = 33.3$, $p<0.001$ between WT and KO, two-way ANOVA)(Fig 5C). However, this phenotype was only seen in adult WT vs adult KO animals. When similar experiments were done in juveniles of both genotype, there was no significant difference in SK currents (SK current for younger WT at +15mV step 61.93 ± 11.9, n= 11 cells; SK current for younger KO at +15mV step 51.2 ± 8.9, n=9 cells; $F_{(1,189)}=0.51$;$p=0.5$; two way ANOVA) (Fig 5D). To delineate the developmental change in SK channels levels between WT and KO, comparisons were made within the same genotype, between different age groups. There was no significant change in the levels of SK currents with age for WT animals (SK current for Older WT at +15mV step 54.2 ± 9, n=13 cells; SK current for younger WT at +15mV step 61.93 ± 11.9, n= 11 cells; $F_{(1,229)}=0.01$, $p=0.9$ two way ANOVA). On the contrary there was a significant increment in levels of SK currents for KO animals as they progressed from juvenile to adult stage (SK current for older KO at +15 mV step 131.73 ± 25.5, n=13 cells; SK current for younger KO at +15mV step 51.2 ± 8.9, n=9 cells; $F_{(1,209)}=21.02$, $p<0.001$; two-way ANOVA).). Together, these observations show that there is an increase in levels of SK currents with age in KO animals, and we note that this correlates with the worsening of spike reliability between adult and juvenile KO animals as described in Fig 3.

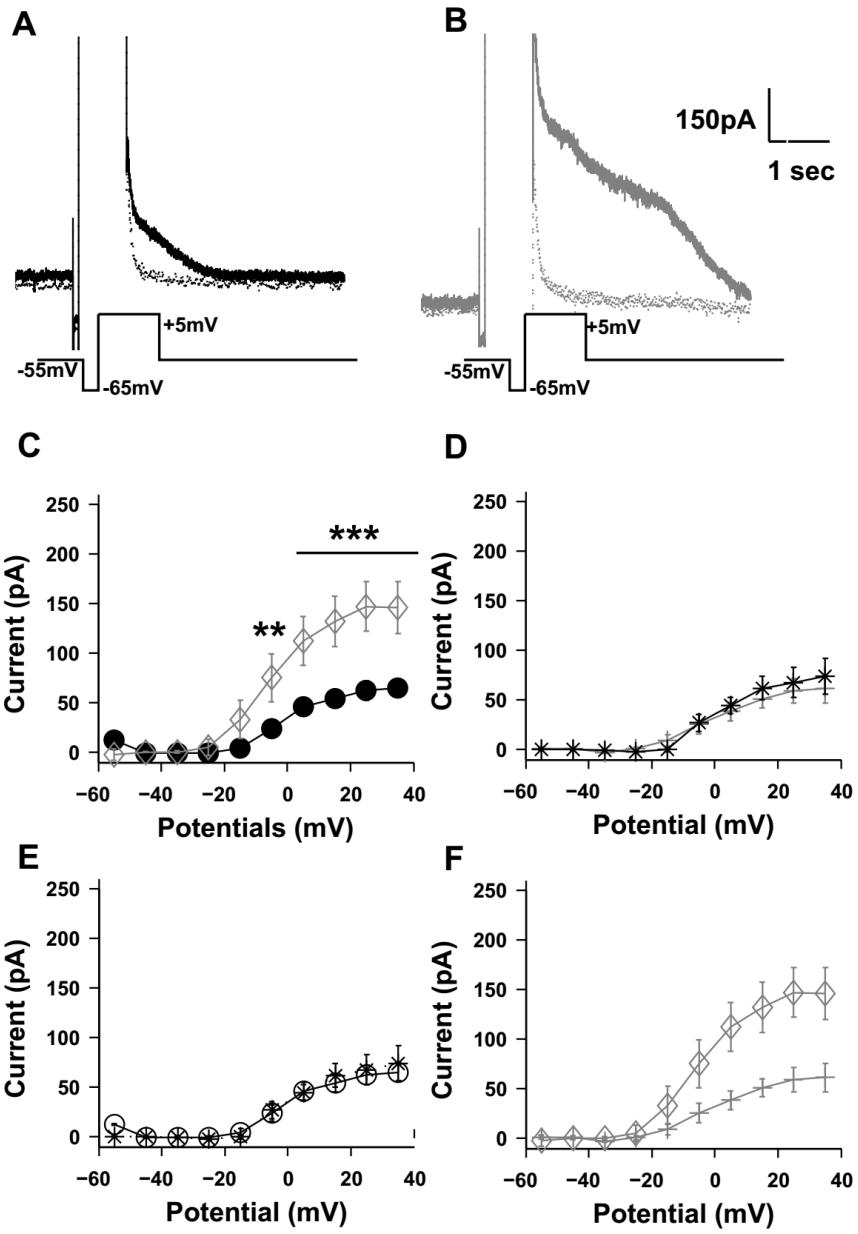

Figure 6. Apamin sensitive SK currents are elevated in KO neurons as compared to WT.

(A) Representative traces showing the outward currents elicited by step depolarization voltage commands in Voltage Clamp, for WT neuron (black) and (B) for KO neuron (grey), pre apamin (solid line) and post apamin (dotted line) perfusion. Trace below indicates command voltage protocol.

(C) IV curve of the apamin sensitive current elicited across multiple steps for WT older cells (n=13 cells, filled black circles) and KO older cells (n=13 cells, grey diamond). Currents are significantly elevated for KO cells as compared to WT cells, for multiple steps. ($F_{(1,240)} = 33.3$, $p<0.001$ between WT and KO, two-way ANOVA, error bars represent SEM)

(D) IV curve of the apamin sensitive current elicited across multiple steps WT younger cells (n=11 cells, black star) and KO younger cells (n=9 cells, grey plus). Currents between KO and WT cells at this age group were not significantly different. ($F_{(1,189)}=0.51$;$p=0.5$; two way ANOVA, error bars represent SEM).

(E) IV curve of the apamin sensitive current elicited across multiple steps for WT younger cells (n=11 cells, black stars) and WT older cells (n=13 cells, black circles). There is no age dependent change in SK currents for WT animals ($F_{(1,229)}=0.01$, $p=0.9$ two way ANOVA,error bars represent SEM).

(F) IV curve of the apamin sensitive current elicited across multiple steps for KO younger cells (n=9 cells, grey plus) and KO older cells (n=13 cells, grey diamonds). There is an age dependent increase in SK currents in KO animals ($F_{(1,209)}=21.02$, $p<0.001$; two-way ANOVA, bars represent SEM).

SK channel expression is unchanged in CA1 and CA3 regions for KO as compared to WT

We have observed that SK current levels are elevated in KO CA1 cells as compared to WT (Fig 6). This elevation might arise due to increase in the levels of SK channels or due to change in SK channel kinetics. The latter might arise due to change in the kinetics of the SK channel itself or due to changes in activity of other

channels which have an effect on SK channels. The putative candidates might be CA2+ channels known to be effected in FXS (Meredith et al., 2007; Ferron et al., 2014,Brown et al., 2001; Contractor et al., 2015). Previous published results have not shown SK channels to be targets of FMRP for transcription regulation, decreasing the likelihood that the levels will be affected in the CA1 region (Darnell et al., 2011; Deng et al., 2018). To specifically test this point, immunofluorescence experiments were used to assess the expression of SK channels. We performed in-situ immunolabeling to measure the intensity of the SK2 isoform in CA3 and CA1 regions of the hippocampus using a specific antibody (Methods, source of reagent) (Fig 7A). We analyzed levels of SK2 protein in different regions and sub sections of the hippocampus for both WT and KO. Similar experiments were done on both adult and juvenile slices. In juvenile animals, we have seen increased number of spikes in CA3 with no significant change in CA1 (Fig 4). However, the levels of SK2 protein was not significantly altered in KO slices for either CA3 (N=4 animals for WT; N=4 animals for KO; $F_{(1,24)}=0.48$; p=0.5 for WT vs KO for CA3; two way ANOVA) (Fig 7B) or CA1 (N=4 animals for WT; N=4 animals for KO; $F_{(1,24)}=0.21$; p=0.6 for WT vs KO for CA1; two way ANOVA) (7C). For adult animals we have seen reduction in spike number in CA1 region (Fig 3E and 3F), but no changes in SK2 levels could be found in either CA1 or CA3 (CA1: N=4 animals for WT; N=4 animals for KO; $F_{(1,24)}=0.25$; p=0.61 for WT vs KO for CA1; two way ANOVA) (Fig 7D) (CA3: N=4 animals for WT; N=4 animals for KO; $F_{(1,24)}=0.3$; p=0.6 for WT vs KO for CA3; two way ANOVA) (Fig 7C). Overall, these labeling studies suggest that the KO does not affect SK expression in either CA1 or CA3. The latter observation is in agreement with previous results (Deng et al., 2018).

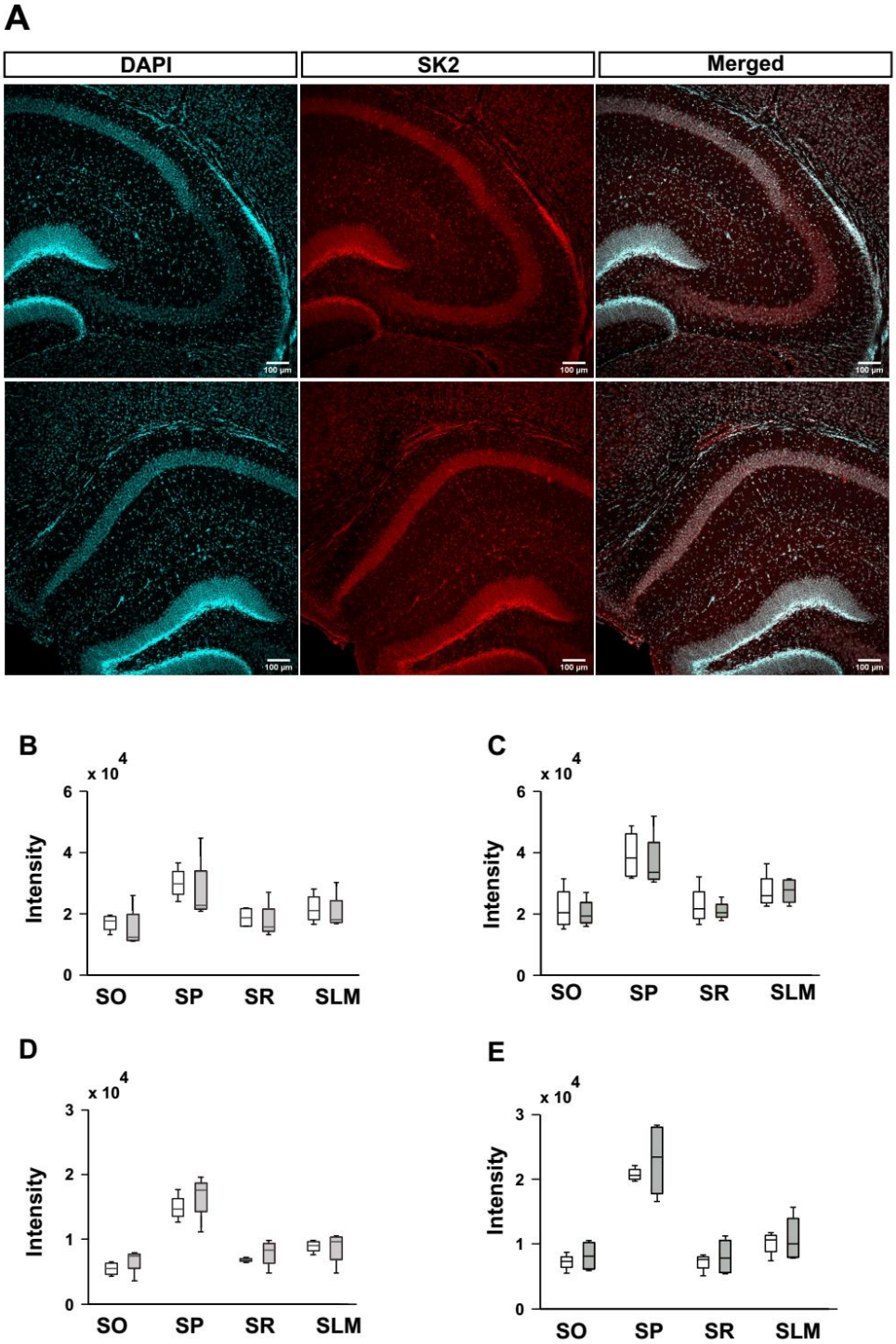

Figure 7. No significant change in SK2 channel levels in KO as compared to WT

A. Representative images of SK2 labeling in CA3 (upper panel) and CA1 (lower panel) for a WT animal. Green false color used for DAPI for better visualization. Scale bar 100µm.

B. Analyzed box plot for mean intensity of SK2 channel in CA3 for juvenile animals. (N=4 animals for WT; N=4 animals for KO; $F_{(1,24)}$=0.48; p=0.5 between WT and KO; two way ANOVA, error bars represent SEM)

C. Analyzed box plot for mean intensity of SK2 channel in CA1 for juvenile animals. (N=4 animals for WT; N=4 animals for KO; $F_{(1,24)}$=0.21; p=0.6 between WT and KO for CA1; two way ANOVA, error bars represent SEM)

D. Analyzed box plot for mean intensity of SK2 channel in CA3 for adult animals. (N=4 animals for WT; N=4 animals for KO; $F_{(1,24)}$=0.3; p=0.6 between WT and KO for CA1, error bars represent SEM)

E. Analyzed box plot for mean intensity of SK2 channel in CA1 for adult animals. (N=4 animals for WT; N=4 animals for KO; $F_{(1,24)}$=0.25; p=0.61 between WT and KO for CA1; two way ANOVA, error bars represent SEM)

Apamin partially rescues the phenotype of increased variability in KO animals

Having shown that elevated and variable SK currents play a role in cellular firing variability, we then asked if blockage of the SK current might rescue the phenotype of increased variability. We observed that WT and KO populations responded differently upon blocking SK currents using apamin. In WT cells, the mean of within cell variability (CV_w) between trials increased (CV_w for WT cells pre

apamin 0.03 ± 0.002, n=13 cells; CV_w for WT cells post apamin 0.04 ± 0.005, n=13 cells) (Fig 6A and 6B). However, for KO cells mean of within cell variability (CV_w) between trials decreased (CV_w for KO cells pre apamin 0.06 ± 0.008, n=13 cells; CV_w for KO cells post apamin 0.05 ± 0.009, n=13 cells) (Fig 6C and 6D). Apamin treatment had no significant affect on within-cell variability (CV_w) for either WT or KO. However, it leads to a partial rescue such that post apamin KO CV_w values were not significantly different from pre apamin WT CV_w values. A complete rescue by apamin would have resulted in reduction of the CV_w of KO cells (which did not happen) as well as a convergence of variability between KO and WT (which did) ($F_{(1,48)}$=0.96 for effect of apamin; $F_{(1,48)}$=0.004 for WT and KO differences; two-way ANOVA with replication). (Fig 6E) We performed similar analysis for between cell (CV_b) variability. Apamin perfusion led to a partial rescue in CV_b parameter as well such that there was a significant reduction in CV_b of KO cells upon apamin perfusion, but no convergence of variability between WT and KO (CV_b for WT cells pre apamin 0.414 ± 0.002; CV_b for WT cells post apamin 0.413 ± 0.002; CV_b for KO cells pre apamin 0.47 ± 0.003; CV_b for KO cells post apamin 0.43 ± 0.002; $F_{(1,96)}$=157.5; p<0.001 for WT and KO differences; $F_{(1,96)}$=53.1; p<0.001 for effect of apamin on CV_b; two-way ANOVA with replication)(Fig 6F). Spike imprecision was also partially rescued with apamin treatment. We found pre treatment spikes were imprecise for KO as compared to WT, but similar to within cell spike variability parameter (CV_w), spike precision did not improve significantly for KO cells upon apamin treatment. (Slope for WT cells pre apamin 0.04 ± 0.004; Slope for WT cells post apamin 0.04 ± 0.004; Slope for KO cells pre apamin 0.07 ± 0.01; Slope for KO cells post apamin 0.06 ± 0.01; $F_{(1, 48)}$=12.8; p=0.0008 for WT and KO differences; $F_{(1,48)}$= 0.04; p=0.84 for effect of apamin; two-way ANOVA with replication). Overall, we find that blockage of

SK currents by apamin partially rescues the variability phenotypes, consistent with our interpretation that elevation in SK currents has a role in variability.

Blocking Calcium has no rescue affect

From the above observations, blocking SK currents led to only a partial rescue in the phenotype of increased imprecision and unreliability for spikes in KO cells. We therefore asked if Ca^{2+}, as an upstream modulator of SK, could also contribute to a partial rescue. To do this we used BAPTA to chelate intracellular Ca^{2+}. We added BAPTA (10mM) into the intracellular recording pipette and assessed spike precision 10 minutes after patching. We found that chelating calcium using BAPTA led to further increase in spike variability instead of rescue. Spike reliability within cell was measured (CV_w) in these experiments and it was found that spikes became significantly more variable post BAPTA than pre BAPTA for both WT and FXS cells (CV_w for WT cells without BAPTA 0.038 ± 0.005, n=30 cells; CV_w for WT cells with BAPTA 0.12 ± 0.02, n=12 cells; $p<0.001$; CV_w for KO cells without BAPTA 0.057 ± 0.006, n=29 cells; CV_w for KO cells with BAPTA 0.16 ± 0.04; $F_{(1,81)}=2.7$; $p=0.1$ for differences between WT and KO;$F_{(1,81)}=40.5$ $p<0.001$ for affect of BAPTA; two way ANOVA) (Fig 6C). Since Ca^{2+} has a large number of ion-channels as other targets, we concluded that it was not a good target for rescue of the variability phenotype.

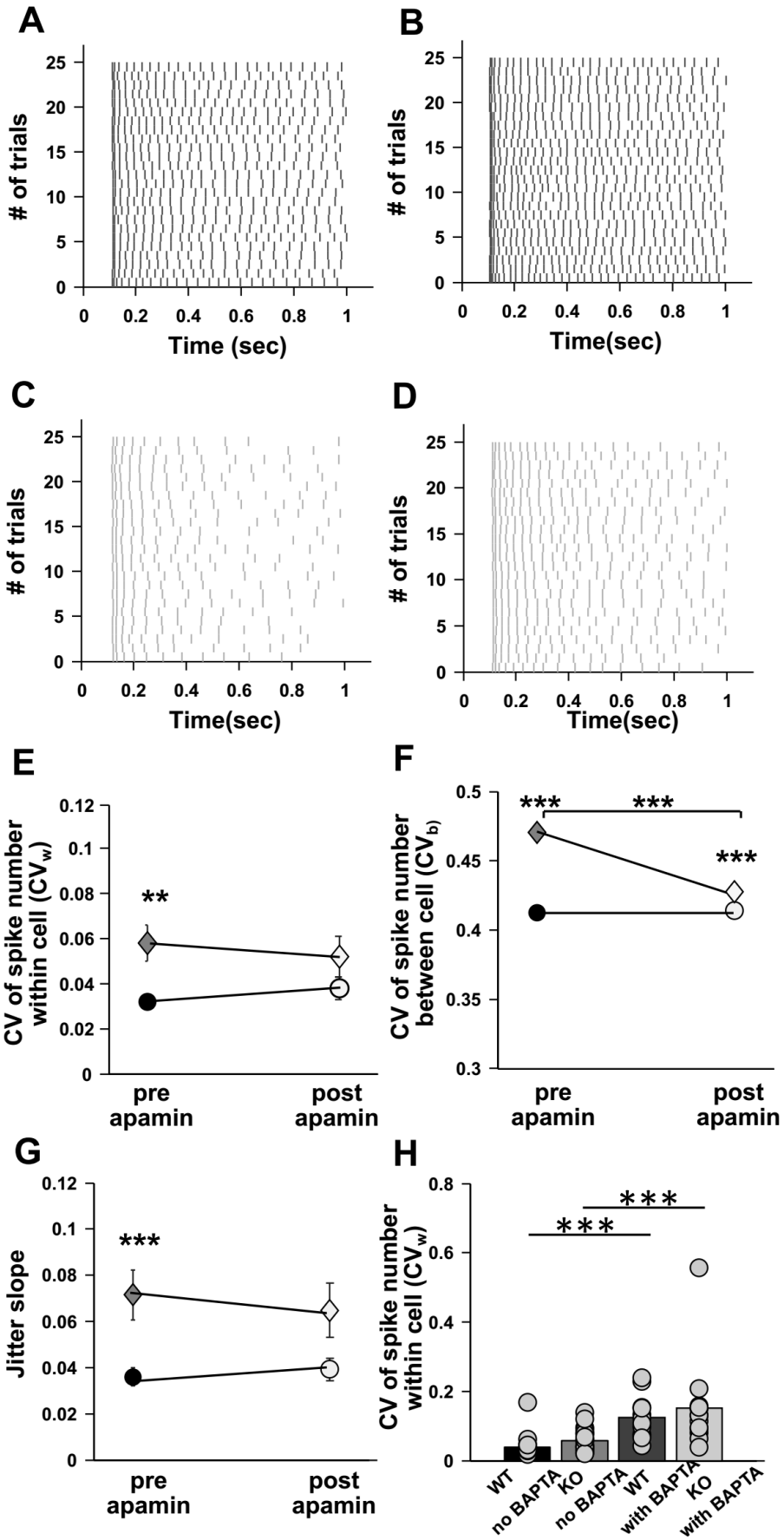
A
B
C
D
E
F
G
H
# of trials
Time (sec)
Time(sec)
CV of spike number within cell (CVw)
CV of spike number between cell (CVb)
Jitter slope
pre apamin
post apamin
WT no BAPTA
KO no BAPTA
WT with BAPTA
KO with BAPTA

630

Figure 8 Partial rescue of within cell variability (CV_w) , between cell variability (CV_b) and spike imprecision in KO neurons upon apamin perfusion.

(A) Representative Raster plot showing spiking for step depolarization protocol for WT, pre apamin.

(B) Representative Raster plot showing spiking for step depolarization protocol for WT, post apamin. Same cell as A.

(C) Representative Raster plot showing spiking for step depolarization protocol for KO, pre apamin.

(D) Representative Raster plot showing spiking for step depolarization protocol for KO, post apamin. Same cell as C.

(E) Change in within cell variability parameter (CV_w) for pre (filled black circles) and post apamin perfusion in WT (n=13 cells, empty black circles) and in KO (n=13 cells, filled grey diamonds for pre apamin and empty grey diamonds for post apamin). There is a partial rescue in CV_w parameter post apamin for KO cells vs. WT cells ($p=0.004$ for WT and KO differences; $p=0.96$ for effect of apamin; two-way ANOVA with replication, error bars represent SEM)

(F) Plot showing change in between cell variability parameter (CV_b) for pre (filled black circles) and post apamin perfusion WT (n=13 cells, empty black circles) and for pre and post apamin perfusion KO (n=13 cells, filled grey diamonds for pre apamin and empty grey diamonds for post apamin). There is a partial rescue in CV_b parameter for KO cells vs. WT cells ($p<0.001$ for WT and KO differences; $p<0.001$

for effect of apamin on CV_b; two way ANOVA with replication, error bars represent SEM).

(G) Plot for jitter slope, a measure of spike precision for pre (filled black circles) and post apamin perfusion WT (n=13 cells, empty black circles) and for pre and post apamin perfusion KO (n=13 cells, filled grey diamonds for pre apamin and empty grey diamonds for post apamin). There is a partial rescue in spike timing precision for KO cells vs. WT cells (p=0.0008 for WT and KO differences; p=0.84 for effect of apamin; two-way ANOVA with replication, error bars represent SEM).

(H) Bar plot showing effect of BAPTA on within cell variability (CV_w) for WT (n=30 cells without BAPTA and n=12 cells with BAPTA) and KO (n=29 cells without BAPTA and n=12 cells with BAPTA). Chelating Ca2+ using BAPTA, lead to a significant increase in spike variability within cell (CV_w) for both WT and KO cells (p=0.1 for differences between WT and KO; p<0.001 for affect of BAPTA; two-way ANOVA with replication, error bars represent SEM).

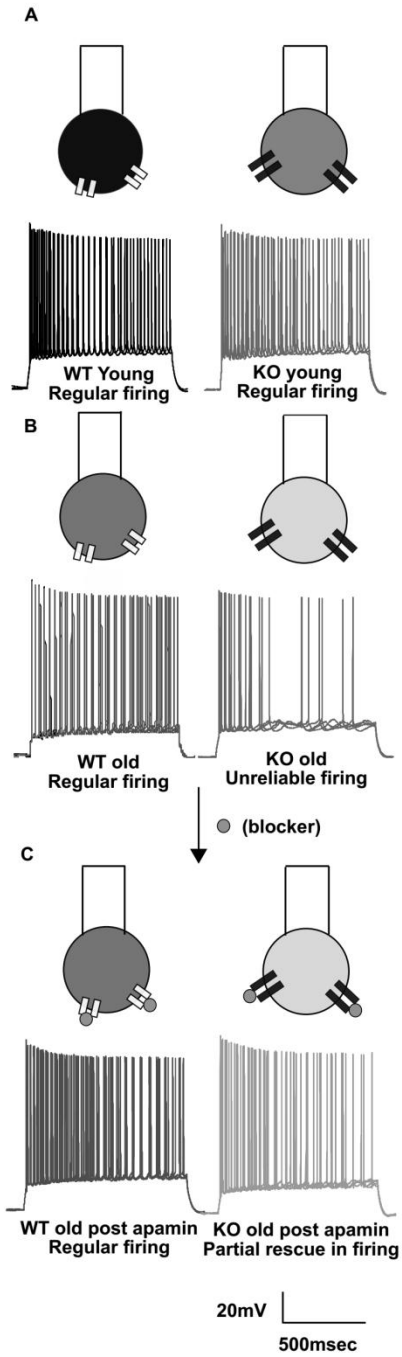

Figure 9 Schematic summary plot indicating developmental increase in spiking variability and the role of SK channels. All spiking traces are actual raw data and show superimposed traces for 4 trials in WT (Dark) and KO (light grey) respectively.

(A) Schematic of neurons, showing Younger WT (Black) and Younger KO (Grey). In young animals we observe precise and reliable spiking across multiple trials. Scale bar 20mV, 500msec.

(B) Schematic of Older WT and Older KO neurons. KO neurons have larger SK currents which are represented by larger icons for SK channels. Noticeably, KO spikes are more variable and less precise especially in the later part of the trial.

(C) Apamin (shown as small grey circles) is used to block SK channels present on soma. Upon apamin perfusion spiking in WT (black) becomes more variable whereas spiking in KO (light grey), increases in frequency leading to increased spike precision and reliability.

Discussion

We have used a mouse model of autism, the fragile X knockout mouse, to investigate cellular correlates of autism in hippocampal CA1 pyramidal neurons. We find that reliability of spiking and spike timing precision is impaired in FXS adult animals. We observed an increase in spiking variability both within a cell over multiple trials and between cells in matching trials, in FXS animals. The variability appeared between 6 and 8 weeks of age, consistent with current understanding of autism as a neurodevelopmental disorder. We observed that the increased spiking variability was accompanied by reduced spiking and elevated mAHP currents. In contrast, we observed increased spiking in CA3 pyramidal cells in juvenile FXS mice

as compared to their WT littermates. We further dissected out the channel contributions to the elevated mAHP and found that SK currents were elevated in adult FXS neurons. However, levels of SK channels were not different between WT and KO mice. To test the hypothesis that elevated SK currents are responsible for unreliable and imprecise spiking in FXS neurons, we used the specific SK blocker apamin and obtained a partial rescue of the phenotype of increased spike variability.

Lowered spike reliability and spike imprecision at cellular intrinsic level in FXS KO hippocampal cells

Our study demonstrates that there is a cell-intrinsic contribution to spiking variability in a mouse model of autism, and implicates over-expression of the SK channel as part of the mechanism. This finding takes significance with the failure of mGluR antagonists and blockers to significantly alleviate FXS symptoms in human patients. These findings point to the likelihood that the mGluR theory (Erickson et al., 2017) may be incomplete. Specifically, our finding of within cell variability and between cell variability in FXS cells shows that cells in the mutant animals may form a heterogeneous population of intrinsically variable neurons, the combined effects of which may lead to network-level incoherence.

This variability in neuronal responses over multiple trials may have implications for multiple behaviors. For example, in learning, the stimulus typically needs to be repeated over multiple trials. If the response of a cell at its intrinsic level as well as between cells is variable, the precision of input spiking as well as output activity would be reduced. This would adversely impact learning rules such as STDP and

associativity (Markram et al., 1997; Bi and Poo, 1998). Further, elevated SK currents will have a direct impact on the recorded sEPSPs at the soma (Ngo-Anh et al., 2005).

SK channel currents elevation may underlie previously observed age dependent changes in KO cellular physiology

FXS has many clinical and experimental attributes of a neurodevelopmental syndrome (Nimchinsky et al., 2001; Cruz-Martin et al., 2010; Meredith et al., 2012). An age-dependent decline in learning has been shown in the drosophila Fragile X model (Choi et al., 2010). Theta Burst Stimulation (TBS) LTP has been showed to produced exaggerated LTP in anterior piriform cortex for older KO mice (12-18 months) but not in younger mice (< 6mths)(Larson, 2005). Similar results were seen in Prefrontal Cortex where TBS produced a significant impairment in LTP for 12 month old mice but not in 2 month old animals (Martin et al., 2016a). Even in humans it has been shown that the males who have a premutation (have CGG repeats <200) predominantly demonstrated fragile-X associated tremor/ataxia syndrome (FXTAS) among patients who were over 50 years old (Cornish et al., 2008). At the molecular level, an age dependent change has also been shown in protein levels in FXS from P17 mice to adults (Tang et al., 2015)

We observed a similar age dependent change in the spike variability phenotype, which was absent in young KO animals, but manifested in older (>6 week) mice (Figure 3C). Age dependent changes in SK channels have been previously reported such that the levels of SK channels are elevated in older animals as compared to

younger ones (Blank et al., 2003). This complements our finding that the AHP difference between WT and KO animals arose in older animals (Fig 4) and that the SK channel underlay the difference in the older animals. There are also evidence of age related changes in Ca2+ levels and Ca2+ uptake mechanisms, such that basal Ca2+ levels are elevated in aging brains (Das and Ghosh, 1996; Kirischuk et al., 1996; Foster and Norris, 1997). Such altered Ca2+ levels would also have a direct impact on the functionality of SK channels. We were not able to directly investigate this possible upstream effect due to the very diverse outcomes of modulating calcium signaling (Figure 6H)

SK channels may be an FMRP target with multiple physiological and behavioral outcomes.

FMRP targets multiple downstream pathways. It not only is a transcription factor but its N-terminus is known to interact with multiple other proteins affecting their functioning (Brown et al., 2010; Deng et al., 2013). Thus mutations in FMRP affect multiple aspects of cellular functioning. Previous RNA-seq results have not shown that SK channels are elevated or affected in FXS (Brown et al., 2001a; Darnell et al., 2011a). However, the functioning of SK currents might be subject to other indirect effects such as changes in Calcium channel distribution, or in their functioning (Meredith et al., 2007; Ferron et al., 2014). Alterations in SK channels have substantial implications for multiple other phenotypes at the cellular and behavioral level. Previous studies have found that FXS KOs have impaired LTP in CA1

hippocampus (Lauterborn et al., 2007; Lee et al., 2012; Tian et al., 2017). We suggest that this impairment might be partially due to elevated SK currents, which are known to shunt EPSPs and also to increase NMDA Mg^{2+} block (Ngo-Anh et al., 2005). Hence our observation of elevated SK currents is consistent with the reported increase LTP threshold in FXS (Lee et al., 2012). These effects on LTP may have knock-on effects on memory phenotypes in FXS models. For example, a mild impairment in learning due to change in platform location in the Morris water maze test has been found in FXS models (D ’hooge et al., 1997; Dobkin et al., 2000).SK currents have been shown to be reduced after learning and this reduction leads decreased variability in spiking events (Sourdet et al., 2003).

Comparison with previously published studies.

Multiple previous studies have found hyper excitability in hippocampus in FXS model mice (Deng and Klyachko, 2016; Luque et al., 2017). We do not find a significant difference between KO and WT f-I curves (Fig 3G and 3H). However, the previously published studies were carried out in the FVB strain of mice and the present study was done on BL/6. Strain dependent differences in FXS have previously been found (Paradee et al., 1999; Dobkin et al., 2000; Lee et al., 2012; Routh et al., 2013). However, (Brager et al., 2012) found a lowering of Input Resistance for KO CA1 cells indicative of reduced excitability. Telias et al 2015 have found similar phenotype as ours in human hippocampal culture cells. In their study, they found that FXS cells were incapable of producing multiple spikes on sustained depolarization at multiple holding potentials, similar to what we observe in this study. It is interesting to note that most excitability analyses and f-I curves use 500 ms current steps, whereas in our study a difference arises after 600 ms, and leads to a reduction in excitability in the KO (Figure 1B and 1G). This suggests that a nuanced interpretation of such

excitability studies is desirable, as the responses may have complex temporal features not reducible to a single measure of excitability. Another important point of difference is the age of the animals. Previous published studies have been done on relatively young animals (<P30) as compared to the present study, where adult animals (6-8 wks) have also been used for the experiments. Our own results (Figure 4B and 4C) show that there is a substantial change in spiking variability as well as AHPs as the animal matures Other studies have also reported an age-dependent effect of expression of plasticity phenotypes in FXS mice (Larson, 2005; Martin et al., 2016). Fragile X Syndrome is known to be a developmental disease where symptoms and many other biochemical and other pathways are known to undergo changes with the age of the animal. Hence it may be important to factor in age-dependence and possibly use a wider range of ages to re-examine some of the conclusions that have been made from FXS models.

Our study is also the first to examine the effect of variability and spiking asynchrony, which again we find to be an age-dependent effect. We postulate that variability in firing of individual cells, which previous studies have not explicitly examined, may be a further complicating factor in analyzing baseline changes arising due to the FMRP mutation.

FMRP KO has different physiological outcomes in different brain regions

In the present study, we make the important and unexpected finding that FMRP KO has differential cell-physiological effects on different sub sections of the same brain region. In an attempt to replicate previous results, we found that there is hyperexcitability in pyramidal neurons of the CA3 region in juvenile mice (as

previously reported, Deng et al 2018) but there was no significant difference in spiking in the CA1 region at the same age. Further, the phenotype reverses for CA1 cells in adult FMRP KO animals such that pyramidal neurons have reduced excitability. Previous studies have given some indication that levels of FMRP are variable in different regions of the brain (Arsenault et. al.; 2016). There is also evidence of hyperconnectivity and hypersynchrony in cortex (Testa-Silva et al., 2012; Gonçalves et al., 2013), which contrasts with poor spike correlations in network activity in hippocampus (Radwan et al., 2016; Arbab et al., 2018, 2018; Talbot et al., 2018). Thus, over multiple readouts, there are now several cases of contradictory outcomes of FXS mutations when examined in different brain regions. Clearly, FXS is a complicated syndrome with multi factorial, differential effects dependent on multiple pathways which might be altered differently in various sub regions of the brain. This raises a general concern about extrapolating results between brain regions in other neurodevelopmental conditions.

Defects in single cell physiology may lead to network and population asynchrony

Multiple studies have shown that variability or lack of coordination in spiking exists in FXS at the network level (Arbab et al., 2018; Talbot et al., 2018). In these tetrode-based studies, variability has been shown at the level of cellular firing patterns in the in-vivo network, hence it is difficult to separate cell-intrinsic properties from synaptic and network phenomena. Clear mechanisms are lacking for this reported asynchrony. However, prior researchers have postulated that synaptic mechanisms may be responsible for the observed asynchrony (Talbot et al., 2018). Our study provides an alternative hypothesis for the mechanism, namely, that the effect is cell-intrinsic and is in part due to altered kinetics of SK channels. Other studies provide

evidence in favor of a role for SK channels in mediating precision and synchronous firing. For example, (Deister et al., 2009), showed that SK channels were responsible for mediating precision in autonomous firing in Globus Pallidus neurons. (Schultheiss et al., 2010) showed that dendritic SK channels also control synchronization. Another study by (Kleiman-Weiner et al., 2009) has shown that SK channels play a role in mediating thalamocortical oscillations. A study by (Combe et al., 2018) shows that SK channels contribute to phase locking for spiking of CA1 cells of the hippocampus to slow gamma frequency inputs from Schaffer Collaterals (SC). Thus, alterations in SK channel kinetics in FXS mutants as established by our study might have substantial impacts on phase coding and synchronization of hippocampal cell populations.

Materials and Methods

Animals

C57BL/6 strain of *Fmr1tmCgr* mouse was used for the experiments. All experimental procedures were approved by the NCBS ethics committee (Project ID: NCBS-IAE-2017/04(N)). The animals were housed in the NCBS animal house where they were maintained in 12 hr light and 12 hr dark cycle. The animals used older animal group was in the range of 6-8 weeks of age, and the younger group was 3-4 weeks old.

Slice preparation

Mice were anaesthetized with halothane. Their head was decapitated after they were euthanized by cervical dislocation. Hippocampal slices were made in the ice cold aCSF of the composition: 115 mM NaCl, 25 mM glucose,25.5 mM $NaHCO_3$, 1.05mM NaH_2PO_4, 3.3mM KCl, 2mM $CaCl_2$, and 1mM $MgCl_2$. 400µm thick slices were made using a VT1200S vibratome and then incubated at room temperature for 1 hour in the aCSF , which was constantly bubbled with 95% O_2 and 5%CO_2. Subsequently, the slices were transferred to the recording chamber where they were maintained at an elevated temperature of 30ºC-34ºC for the recordings.

Electrophysiology

CA1 neurons were identified under an upright DIC microscope (Olympus BX1WI microscope) using a 40X objective (water immersion lens, 0.9 NA LUMPLFLN, 40X). 2-4 MOhm pipettes were pulled from thick walled borosilicate glass capillaries on a P-1000 Flaming micropipette puller (Sutter instruments). The pipettes were filled with internal solution of the following composition for whole cell Current Clamp recordings: 120mM potassium gluconate, 20mM KCl, 0.2mM EGTA, 4mM NaCl,10mM HEPES buffer, 10mM phosphocreatine, 4mM Mg-ATP, and 0.3mM Na-GTP (pH 7.4, 295 mOsm). For Voltage Clamp recordings, the same composition of internal solution was used with the one change that 120mM potassium gluconate was substituted with 120mM potassium methylsulphate. Cells were recorded if they had a resting potential <-60mV. We also required that they exhibit stable firing with little or no depolarization block for lower current inputs. Series resistance and input resistance were continuously monitored during the protocols and the cell was discarded if these parameters changed by >25%.

Protocol for measuring spike variability and analysis

A step input current stimulus of 150pA DC for 900 ms was used for the majority of the recordings. In some cases, as indicated in the text, frozen noise and sinusoidal input currents were also used, riding on a baseline current step of 150pA, and again for a duration of 900 ms. SD of noise used in noise protocols were 10pA, 25pA, 50pA and 100pA with a time-cutoff of τ=3msec. For sinusoidal currents SD of 50pA and 100pA were used at 5 Hz. All the protocols were repeated for 25 trials. Within cell spike variability (CV_w) was computed as Coefficient of Variation (CV) in spike numbers across 25 trials. Spike numbers computed for all 25 trials were used to find Standard Deviation in spike numbers which is then divided by mean number of spikes to find CV. CV_w, the within-cell variability, was computed as the Coefficient of Variation (CV) between trials of each given cell.For computing between cell spikes variability (CV_b) spike numbers were analyzed across different cells by matching individual trials.

Measurement of spike timing precision

Spike time precision for the step input protocol was measured as Standard Deviation (SD) in the timing of the spikes. Spike times were found for all the spikes, produced by a cell, for all the trials. Further, spike time jitter was calculated for spikes by comparing SD in spike times for a given spike number (Fig 1B and Fig 1G).

AHP measurement

AHPs were measured by holding the cell at -70mV in Current Clamp mode, using some holding current. In each trial, the holding current was set to zero for 200msec and then step input for 100msec was delivered. The current during this step input

was adjusted so that the cell produced 5 spikes in 100msec. This stimulus was repeated for 15 trials and the voltage traces of all the trials were averaged. AHPs were analyzed as the hyperpolarization after the spike train. mAHP was computed as the average hyperpolarization 50msec after the spike train, and sAHP was computed 200msec after the spike train (Fig 4A and 4B).

Immunofluorescense experiments and analysis

3-4 week or 6-8 week old animals were anaesthetized and brains were dissected out. Brains were fixed in 4%PFA for 48hrs at 4°C. Post fixation, brains were washed with PBS and 30 µm thick slices were cut on a VT12000S vibratome. Slices were kept in cryoprotectant solution and stored at -20°C for further use. Slices were re-suspended in Phosphate Buffer Saline (PBS) solution for the experiment. 50mM Ammonium Chloride (NH_4Cl) was used to quench auto fluorescence from the samples. After multiple steps of washing and permeabilization with 0.3% PBS with Triton-X 100, cells were incubated with 5% Normal Goat Serum (NGS) for blocking for 1-2 hr. Followed by washes slices were incubated in primary antibody for SK2 channel, overnight at 4°C. Primary antibody was purchased from Alomone Labs and were used in 1:300 dilution with 2.5% NGS. Further, slices were incubated in secondary antibody at 1:500 dilution for 1-2 hrs at room temperature. Followed by several washes and DAPI stain (Sigma) for 15 mins in PBS, slices were mounted in Prolong Gold mounting media and imaged in Olympus FV3000 confocal microscope.

For measuring M and I_h currents

For measuring Ih sag current, cells were held at -70mV and given a step hyperpolarization of 250pA for 500msec. Sag current was calculated by the finding the percentage change between maximum and steady state voltages during the

hyperpolarizing pulse $((V_{max}-V_{ss})/V_{max})/100$. Each cell was presented with 15 trials and I_h sag was averaged across all the trials to get a value for a cell.

TTX (0.5 µM) was added in the bath while measuring M currents in voltage-clamp. For measuring M currents, cells were held at -20mV and M currents were deactivated in steps from -20mV to -80mV in difference of 10mV of 900msec time duration. Difference between steady state current after the start of the protocol (from the last 250msec) and baseline of the cell was quantified as the current elicited due to the protocol. Specific M current blocker XE991 (30µM) was perfused to get post toxin trace. Difference between Pre and Post XE991 was quantified as M current.

For measuring SK currents

TTX (0.5 µM) was added in the bath while measuring SK currents in voltage-clamp. For measuring SK currents cells were held at -55mV while increasing voltage steps were given from -55mV to +35mV, in increments of 10mV, for 800msec duration. Each voltage step was preceded with a small hyperpolarization from -55mV to -65mV for 100msec. Cell capacitance compensation was done during the recordings. The SK currents were estimated from the amplitude of the outward current 25 ms after the voltage was returned to the holding potential as the initial part of the trace will be contaminated with capacitance currents (Figure 5A and 5B). Apamin perfusion (100nM) was done to identify these currents. Same protocol was used post apamin perfusion. The difference current of pre apamin and post apamin was quantified to find apamin sensitive SK current.

Data acquisition and Analysis

Recordings were done using an Axopatch 200 B amplifier and digitized using Digidata 1400A. Current clamp recordings were filtered at 10KHz and sampled at 20KHz. Voltage Clamp recordings were carried out at a gain of 5, filtered at 3 KHz, sampled at 20KHz. All analysis was done using custom written code in Matlab(R2013a) and Graph Pad Prism 6. Statistical tests were done after checking the normality of the data. We used a Kolmogorov-Smirnoff test for normality. If this indicated that the data was non-normal, we carried out the significance analysis using Wilcoxon rank sum rank sum test. All the data is plotted as mean ± SEM.

Drugs and Chemicals used

All toxins were purchased from Sigma other than TTX which was from Hello Bio. TTX (Stock of 0.5mM) and apamin (Stock solution of 1mM) were made in milliQ water. XE991 (Stock 10mM) was made in DMSO. All stocks were stored at -20° C and were diluted to the working concentration immediately before the experiments.

Experiment design and statistical analysis

We have used hippocampal slice preparation in this study, where CA1 region was used for electrical recordings. Different current inputs were injected into the cell soma via recording electrode and elicited spikes were recorded in current clamp mode. Spiking variability was assessed by finding Coefficient of Variation (CV) for within cell and between cells. Spike precision was assessed by finding slope of Standard deviation in spike times over multiple trials. SK currents were measured in voltage clamp and were found to be partially responsible for increased variability. All analysis and plotting was done in MATLAB. Normality of the data was checked and if found to be not normal, non parametric tests were done.

References

Arbab T, Battaglia FP, Pennartz CMA, Bosman CA (2018a) Abnormal hippocampal theta and gamma hypersynchrony produces network and spike timing disturbances in the Fmr1-KO mouse model of Fragile X syndrome. Neurobiol Dis 114:65–73 Available at: https://doi.org/10.1016/j.nbd.2018.02.011.

Arbab T, Battaglia FP, Pennartz CMA, Bosman CA (2018b) Abnormal hippocampal theta and gamma hypersynchrony produces network and spike timing disturbances in the Fmr1-KO mouse model of Fragile X syndrome. Neurobiol Dis.

Arbab T, Pennartz CMA, Battaglia FP (2018c) Impaired hippocampal representation of place in the Fmr1-knockout mouse model of fragile X syndrome. Sci Rep.

Bi G, Poo M (1998) Synaptic Modifications in Cultured Hippocampal Neurons : Dependence on Spike Timing , Synaptic Strength , and Postsynaptic Cell Type. 18:10464–10472.

Blank T, Nijholt I, Kye MJ, Radulovic J, Spiess J (2003) Small-conductance, Ca2+-activated K+channel SK3 generates age-related memory and LTP deficits. Nat Neurosci 6:911–912.

Brager DH, Akhavan AR, Johnston D (2012) Impaired Dendritic Expression and Plasticity of h-Channels in the fmr1-/yMouse Model of Fragile X Syndrome. Cell Rep.

Brown MR, Kronengold J, Gazula VR, Chen Y, Strumbos JG, Sigworth FJ, Navaratnam D, Kaczmarek LK (2010) Fragile X mental retardation protein controls gating of the sodium-activated potassium channel Slack. Nat Neurosci.

Brown V, Jin P, Ceman S, Darnell JC, Donnell WTO, Tenenbaum SA, Jin X, Feng Y, Wilkinson KD, Keene JD, Darnell RB, Warren ST, Carolina N (2001a) Microarray Identification of FMRP-Associated Brain mRNAs and Altered mRNA Translational Profiles in Fragile X Syndrome. 107:477–487.

Brown V, Jin P, Ceman S, Darnell JC, O'donnell WT, Tenenbaum SA, Jin X, Feng Y, Wilkinson KD, Keene JD, Darnell RB, Warren ST (2001b) Microarray Identification of FMRP-Associated Brain mRNAs and Altered mRNA Translational Profiles in Fragile X Syndrome Howard Hughes Medical Institute Department of Human Genetics FMRP is largely cytoplasmic, incorporated into large messenger-ribonucleopr. Available at: http://www.cell.com/cgi/content/full/107/4/.

Carandini M (2004) Amplification of Trial-to-Trial Response Variability by Neurons in Visual Cortex. 2.

Carlen PL (1997) Reversible inhibition of I K , I AHP , I h and I Ca currents by internally applied gluconate in rat hippocampal pyramidal neurones. :343–350.

Choi CH, McBride SMJ, Schoenfeld BP, Liebelt DA, Ferreiro D, Ferrick NJ, Hinchey P, Kollaros M, Rudominer RL, Terlizzi AM, Koenigsberg E, Wang Y, Sumida A, Nguyen HT, Bell AJ, McDonald T V., Jongens TA (2010a) Age-dependent

cognitive impairment in a Drosophila Fragile X model and its pharmacological rescue. Biogerontology.

Choi CH, McBride SMJ, Schoenfeld BP, Liebelt DA, Ferreiro D, Ferrick NJ, Hinchey P, Kollaros M, Rudominer RL, Terlizzi AM, Koenigsberg E, Wang Y, Sumida A, Nguyen HT, Bell AJ, McDonald T V., Jongens TA (2010b) Age-dependent cognitive impairment in a Drosophila Fragile X model and its pharmacological rescue. Biogerontology 11:347–362.

Combe CL, Canavier CC, Gasparini S (2018) Intrinsic mechanisms of frequency selectivity in the proximal dendrites of CA1 pyramidal neurons. J Neurosci 38:0449–18 Available at: http://www.jneurosci.org/lookup/doi/10.1523/JNEUROSCI.0449-18.2018.

Contractor A, Klyachko VA, Portera-Cailliau C (2015a) Altered Neuronal and Circuit Excitability in Fragile X Syndrome. Neuron.

Contractor A, Klyachko VA, Portera-Cailliau C (2015b) Altered Neuronal and Circuit Excitability in Fragile X Syndrome. Neuron 87:699–715 Available at: http://dx.doi.org/10.1016/j.neuron.2015.06.017.

Cornish KM, Li L, Kogan CS, Jacquemont S, Turk J, Dalton A, Hagerman RJ, Hagerman PJ (2008a) Age-dependent cognitive changes in carriers of the fragile X syndrome. Cortex 44:628–636.

Cornish KM, Li L, Kogan CS, Jacquemont S, Turk J, Dalton A, Hagerman RJ, Hagerman PJ (2008b) Age-dependent cognitive changes in carriers of the fragile X syndrome. Cortex.

Crook SM, Ermentrout GB, Bower JM (1998) Spike Frequency Adaptation Affects

the Synchronization Properties of Networks of Cortical Oscillators. Neural Comput.

Cruz-Martin A, Crespo M, Portera-Cailliau C (2010) Delayed Stabilization of Dendritic Spines in Fragile X Mice. J Neurosci 30:7793–7803 Available at: http://www.jneurosci.org/cgi/doi/10.1523/JNEUROSCI.0577-10.2010.

Cudmore RH, Fronzaroli-Molinieres L, Giraud P, Debanne D (2010) Spike-Time Precision and Network Synchrony Are Controlled by the Homeostatic Regulation of the D-Type Potassium Current. J Neurosci 30:12885–12895 Available at: http://www.jneurosci.org/cgi/doi/10.1523/JNEUROSCI.0740-10.2010.

D ’hooge R, Nagels G, Franck F, Bakker CE, Reyniers # E, Storm K, Kooy RF, Oostra BA, Willems: PJ, De Deyn PP (1997) MILDLY IMPAIRED WATER MAZE PERFORMANCE IN MALE Fmrl KNOCKOUT MICE. ~ Pergamon Neurosci 76:367–376.

Darnell JC, Driesche SJ Van, Zhang C, Ying K, Hung S, Mele A, Fraser CE, Stone EF, Chen C, Fak JJ, Chi SW, Licatalosi DD, Richter JD, Darnell RB (2011a) FMRP Stalls Ribosomal Translocation on mRNAs Linked to Synaptic Function and Autism. Cell 146:247–261 Available at: http://dx.doi.org/10.1016/j.cell.2011.06.013.

Darnell JC, Van Driesche SJ, Zhang C, Hung KYS, Mele A, Fraser CE, Stone EF, Chen C, Fak JJ, Chi SW, Licatalosi DD, Richter JD, Darnell RB (2011b) FMRP stalls ribosomal translocation on mRNAs linked to synaptic function and autism. Cell.

Das N, Ghosh S (1996) The effect of age on calcium dynamics in rat brain in vivo. Mech Ageing Dev.

Deister CA, Chan CS, Surmeier DJ, Wilson CJ (2009) Calcium-Activated SK Channels Influence Voltage-Gated Ion Channels to Determine the Precision of Firing in Globus Pallidus Neurons. J Neurosci.

Deng P-Y, Sojka D, Klyachko VA (2011) Abnormal Presynaptic Short-Term Plasticity and Information Processing in a Mouse Model of Fragile X Syndrome. J Neurosci.

Deng P, Carlin D, Oh YM, Myrick LK, Warren ST, Cavalli V, Klyachko VA (2018) Voltage-Independent SK Channel Dysfunction Causes Neuronal Hyperexcitability in the Hippocampus of Fmr1 KO mice Voltage-Independent SK Channel Dysfunction Causes Neuronal Hyperexcitability in the Hippocampus of Fmr1 KO mice Abbreviated Title : SK Channel .

Deng PY, Klyachko VA (2016) Increased Persistent Sodium Current Causes Neuronal Hyperexcitability in the Entorhinal Cortex of Fmr1 Knockout Mice. Cell Rep.

Deng PY, Rotman Z, Blundon JA, Cho Y, Cui J, Cavalli V, Zakharenko SS, Klyachko VA (2013) FMRP Regulates Neurotransmitter Release and Synaptic Information Transmission by Modulating Action Potential Duration via BK Channels. Neuron.

Dobkin C, Rabe A, Dumas R, El Idrissi A, Haubenstock H, Ted Brown W (2000) Fmr1 knockout mouse has a distinctive strain-specific learning impairment. Neuroscience.

Erickson CA, Davenport MH, Schaefer TL, Wink LK, Pedapati E V., Sweeney JA, Fitzpatrick SE, Brown WT, Budimirovic D, Hagerman RJ, Hessl D, Kaufmann WE, Berry-Kravis E (2017) Fragile X targeted pharmacotherapy: Lessons learned and future directions. J Neurodev Disord 9:1–14.

Faisal AA, Selen LPJ, Wolpert DM (2008) Noise in the nervous system. Nat Rev Neurosci.

Ferron L, Nieto-Rostro M, Cassidy JS, Dolphin AC (2014a) Fragile X mental retardation protein controls synaptic vesicle exocytosis by modulating N-type calcium channel density. Nat Commun.

Ferron L, Nieto-Rostro M, Cassidy JS, Dolphin AC (2014b) Fragile X mental retardation protein controls synaptic vesicle exocytosis by modulating N-type calcium channel density. Nat Commun 5:1–14 Available at: http://dx.doi.org/10.1038/ncomms4628.

Foster TC, Norris CM (1997) Age-associated changes in ca2+-dependent processes: Relation to hippocampal synaptic plasticity. Hippocampus.

Fricker D, Miles R (2000) EPSP amplification and the precision of spike timing in hippocampal neurons. Neuron.

Fujisawa S, Yamada MK, Nishiyama N, Matsuki N, Ikegaya Y (2004) BDNF boosts spike fidelity in chaotic neural oscillations. Biophys J 86:1820–1828 Available at: http://dx.doi.org/10.1016/S0006-3495(04)74249-6.

Gabbiani F, Dewell R (2018) M-current regulates firing mode and spike reliability in a collision detecting neuron. bioRxiv:335174 Available at: https://www.biorxiv.org/content/early/2018/05/31/335174.

Gastrein P, Campanac É, Gasselin C, Cudmore RH, Bialowas A, Carlier E, Fronzaroli-Molinieres L, Ankri N, Debanne D (2011) The role of hyperpolarization-activated cationic current in spike-time precision and intrinsic resonance in cortical neurons in vitro. J Physiol.

Gittelman JX (2006) Kv1.1-Containing Channels Are Critical for Temporal Precision During Spike Initiation. J Neurophysiol 96:1203–1214 Available at: http://jn.physiology.org/cgi/doi/10.1152/jn.00092.2005.

Gonçalves JT, Anstey JE, Golshani P, Portera-Cailliau C (2013) Circuit level defects in the developing neocortex of Fragile X mice. Nat Neurosci.

Gross C, Yao X, Pong DL, Jeromin A, Bassell GJ (2011) Fragile X mental retardation protein regulates protein expression and mRNA translation of the potassium channel Kv4.2. J Neurosci 31:5693–5698.

Guan D, Higgs MH, Horton LR, Spain WJ, Foehring RC (2011) Contributions of Kv7-mediated potassium current to sub- and suprathreshold responses of rat layer II/III neocortical pyramidal neurons. J Neurophysiol 106:1722–1733 Available at: http://jn.physiology.org/cgi/doi/10.1152/jn.00211.2011.

Han X, Boyden ES (2007) Multilpe-color optical activation, silencing, and desynchronization of neural activity, with single-spike temporal resolution. PLoS One 2.

Hönigsperger C, Marosi M, Murphy R, Storm JF (2015) Dorsoventral differences in Kv7/M-current and its impact on resonance, temporal summation and excitability in rat hippocampal pyramidal cells. J Physiol.

Hou GQ, Pan X, Liao CS, Wang SH, Li DF (2012) SK channels modulate the excitability and firing precision of projection neurons in the robust nucleus of the arcopallium in adult male zebra finches. Neurosci Bull.

Kirischuk S, Voitenko N, Kostyuk P, Verkhratsky A (1996) Age-associated changes of cytoplasmic calcium homeostasis in cerebellar granule neurons in situ:

Investigation on thin cerebellar slices. Exp Gerontol.

Kleiman-Weiner M, Beenhakker MP, Segal WA, Huguenard JR (2009) Synergistic Roles of GABA A Receptors and SK Channels in Regulating Thalamocortical Oscillations. J Neurophysiol 102:203–213 Available at: www.jn.org.

Kwag J, Jang HJ, Kim M, Lee S (2014) M-type potassium conductance controls the emergence of neural phase codes: A combined experimental and neuron modelling study. J R Soc Interface.

Larson J (2005) Age-Dependent and Selective Impairment of Long-Term Potentiation in the Anterior Piriform Cortex of Mice Lacking the Fragile X Mental Retardation Protein. J Neurosci.

Lauterborn JC, Rex CS, Krama E, Chen LY, Pandyarajan V, Lynch G, Gall CM (2007) Brain-Derived Neurotrophic Factor Rescues Synaptic Plasticity in a Mouse Model of Fragile X Syndrome. 27:10685–10694.

Lee HY, Ge W-P, Huang W, He Y, Wang GX, Rowson-Baldwin A, Smith SJ, Jan YN, Jan LY (2011) Bidirectional Regulation of Dendritic Voltage-Gated Potassium Channels by the Fragile X Mental Retardation Protein. Neuron 72:1091.

Lee HY, Ge W, Huang W, He Y, Wang GX, Smith SJ, Jan YN, Jan LY (2012) Bidirectional Regulation of Dendritic Voltage-gated Potassium Channels by the Fragile X Mental Retardation Protein. Neuron 72:630–642.

Lubs' HA (n.d.) A Marker X Chromosome.

Luque MA, Beltran-matas P, Marin MC, Torres B, Herrero L (2017) Excitability is increased in hippocampal CA1 pyramidal cells of Fmr1 knockout mice. :1–18.

Madison D V, Lancaster B, Nicoll RA (1987) Voltage Clamp Analysis of Cholinergic

Action in the Hippocampus. 7:733–741.

Markram H, Lu J, Frotscher M, Sakmann B (1997) Regulation of Synaptic Efficacy by Coincidence of Postsynaptic APs and EPSPs. 275:213–215.

Martin HGS, Lassalle O, Brown JT, Manzoni OJ (2016a) Age-Dependent Long-Term Potentiation Deficits in the Prefrontal Cortex of the Fmr1 Knockout Mouse Model of Fragile X Syndrome. Cereb Cortex 26:2084–2092.

Martin HGS, Lassalle O, Brown JT, Manzoni OJ (2016b) Age-Dependent Long-Term Potentiation Deficits in the Prefrontal Cortex of the Fmr1 Knockout Mouse Model of Fragile X Syndrome. Cereb Cortex.

Meredith RM, Dawitz J, Kramvis I (2012) Sensitive time-windows for susceptibility in neurodevelopmental disorders. Trends Neurosci 35:335–344 Available at: http://dx.doi.org/10.1016/j.tins.2012.03.005.

Meredith RM, Holmgren CD, Weidum M, Burnashev N (2007) Article Increased Threshold for Spike-Timing-Dependent Plasticity Is Caused by Unreliable Calcium Signaling in Mice Lacking Fragile X Gene Fmr1. :627–638.

Ngo-Anh TJ, Bloodgood BL, Lin M, Sabatini BL, Maylie J, Adelman JP (2005) SK channels and NMDA receptors form a Ca2+-mediated feedback loop in dendritic spines. Nat Neurosci.

Nigro MJ, Mateos-Aparicio P, Storm JF (2014) Expression and Functional Roles of Kv7/KCNQ/M-Channels in Rat Medial Entorhinal Cortex Layer II Stellate Cells. J Neurosci 34:6807–6812 Available at: http://www.jneurosci.org/cgi/doi/10.1523/JNEUROSCI.4153-13.2014.

Nimchinsky E a, Oberlander a M, Svoboda K (2001) Abnormal development of

dendritic spines in FMR1 knock-out mice. J Neurosci 21:5139–5146.

O'Donnell WT, Warren ST (2002) A Decade of Molecular Studies of Fragile X Syndrome. Annu Rev Neurosci.

Orban G, Kiss T, Erdi P (2006) Intrinsic and Synaptic Mechanisms Determining the Timing of Neuron Population Activity During Hippocampal Theta Oscillation. J Neurophysiol 96:2889–2904 Available at: http://jn.physiology.org/cgi/doi/10.1152/jn.01233.2005.

Paradee W, Melikian HE, Rasmussen DL, Kenneson A, Conn PJ (1999) FRAGILE X MOUSE : STRAIN EFFECTS OF KNOCKOUT PHENOTYPE AND EVIDENCE SUGGESTING DEFICIENT AMYGDALA FUNCTION. 94:185–192.

Pfeuty B, Mato G, Golomb D, Hansel D (2003) Electrical synapses and synchrony: the role of intrinsic currents. J Neurosci 23:6280–6294 Available at: http://www.ncbi.nlm.nih.gov/pubmed/12867513.

Radwan B, Dvorak D, Fenton AA (2016) Impaired cognitive discrimination and discoordination of coupled theta-gamma oscillations in Fmr1 knockout mice. Neurobiol Dis 88:125–138 Available at: http://dx.doi.org/10.1016/j.nbd.2016.01.003.

Routh BN, Johnston D, Brager DH (2013) Loss of functional A-type potassium channels in the dendrites of CA1 pyramidal neurons from a mouse model of fragile X syndrome. J Neurosci 33:19442–19450 Available at: http://www.ncbi.nlm.nih.gov/pubmed/24336711.

Sah P, Clements JD (1999) Photolytic Manipulation of [Ca 2 ⁄+] i Reveals Slow Kinetics of Potassium Channels Underlying the Afterhyperpolarization in

Hipppocampal Pyramidal Neurons. 19:3657–3664.

Schultheiss NW, Edgerton JR, Jaeger D (2010) Phase Response Curve Analysis of a Full Morphological Globus Pallidus Neuron Model Reveals Distinct Perisomatic and Dendritic Modes of Synaptic Integration. J Neurosci.

Sourdet V, Russier M, Daoudal G, Ankri N, Debanne D (2003) Long-Term Enhancement of Neuronal Excitability and Temporal Fidelity Mediated by Metabotropic Glutamate Receptor Subtype 5.

Stevens CF, Zador a M (1998) Input synchrony and the irregular firing of cortical neurons. Nat Neurosci 1:210–217 Available at: http://www.ncbi.nlm.nih.gov/pubmed/10195145.

Strumbos JG, Brown MR, Kronengold J, Polley DB, Kaczmarek LK (2010) Fragile X Mental Retardation Protein Is Required for Rapid Experience-Dependent Regulation of the Potassium Channel Kv3 . 1b. 30:10263–10271.

Talbot ZN, Sparks FT, Dvorak D, Curran BM, Alarcon JM, Fenton AA (2018a) Normal CA1 Place Fields but Discoordinated Network Discharge in a Fmr1-Null Mouse Model of Fragile X Syndrome. Neuron:684–697.

Talbot ZN, Sparks FT, Dvorak D, Curran BM, Alarcon JM, Fenton AA (2018b) Normal CA1 Place Fields but Discoordinated Network Discharge in a Fmr1-Null Mouse Model of Fragile X Syndrome. Neuron.

Tang B, Wang T, Wan H, Han L, Qin X, Zhang Y, Wang J, Yu C, Berton F, Francesconi W, Yates JR, Vanderklish PW, Liao L (2015) *Fmr1* deficiency promotes age-dependent alterations in the cortical synaptic proteome. Proc Natl Acad Sci 112:E4697–E4706 Available at:

http://www.pnas.org/lookup/doi/10.1073/pnas.1502258112.

Testa-Silva G, Loebel A, Giugliano M, De Kock CPJ, Mansvelder HD, Meredith RM (2012) Hyperconnectivity and slow synapses during early development of medial prefrontal cortex in a mouse model for mental retardation and Autism. Cereb Cortex 22:1333–1342.

Tian Y, Yang C, Shang S, Cai Y, Deng X, Zhang J, Shao F, Zhu D, Liu Y, Chen G, Liang J, Sun Q, Qiu Z, Zhang C (2017) Loss of FMRP Impaired Hippocampal Long-Term Plasticity and Spatial Learning in Rats. Front Mol Neurosci 10:1–14 Available at: http://journal.frontiersin.org/article/10.3389/fnmol.2017.00269/full.

Zhu P, Li J, Zhang L, Liang Z, Tang B, Liao WP, Yi YH, Su T (2018) Development-related aberrations in Kv1.1 α-subunit exert disruptive effects on bioelectrical activities of neurons in a mouse model of fragile X syndrome. Prog Neuro-Psychopharmacology Biol Psychiatry 84:140–151 Available at: https://doi.org/10.1016/j.pnpbp.2018.02.011.

Acknowledgements

DD was funded by NCBS/TIFR Intramural funds during the project. I would like to acknowledge National Mouse Resource (NaMoR) and Department of Biotechnology (DBT) for providing funds for mouse maintenance and experimental equipments. I would like to thank Suranjana Pal, Bishal Basak, Vidya Ramesh, Sarfaraz Nawaz, Mohammed Shariq, Dipannita Sarkar for help with Immunofluorescence experiments. I would also thank Giselle Fernandes, Shreya Das Sharma, Aviral

Goel, Sathyaa Subramaniyam, Aanchal Bhatia and Sahil Moza for useful inputs from time to time.